Extraction of Vessel Acoustic Source Levels and Total Sound Exposure Levels from Passive Acoustic Recordings on the Eastern Nova Scotian Shelf Slope and in the Gully Marine Protected Area

N.A. Cochrane and H.B. Moors-Murphy

Department of Fisheries & Oceans
Maritimes Region
Ocean and Ecosystem Sciences Division
Bedford Institute of Oceanography
PO Box 1006
Dartmouth, NS
B2Y 4A2

2017

Canadian Technical Report of Fisheries and Aquatic Sciences 3237

Fisheries and Oceans Canada | Pêches et Océans Canada

Canada

Canadian Technical Report of Fisheries and Aquatic Sciences

Technical reports contain scientific and technical information that contributes to existing knowledge but which is not normally appropriate for primary literature. Technical reports are directed primarily toward a worldwide audience and have an international distribution. No restriction is placed on subject matter and the series reflects the broad interests and policies of Fisheries and Oceans Canada, namely, fisheries and aquatic sciences.

Technical reports may be cited as full publications. The correct citation appears above the abstract of each report. Each report is abstracted in the data base *Aquatic Sciences and Fisheries Abstracts*.

Technical reports are produced regionally but are numbered nationally. Requests for individual reports will be filled by the issuing establishment listed on the front cover and title page.

Numbers 1-456 in this series were issued as Technical Reports of the Fisheries Research Board of Canada. Numbers 457-714 were issued as Department of the Environment, Fisheries and Marine Service, Research and Development Directorate Technical Reports. Numbers 715-924 were issued as Department of Fisheries and Environment, Fisheries and Marine Service Technical Reports. The current series name was changed with report number 925.

Rapport technique canadien des sciences halieutiques et aquatiques

Les rapports techniques contiennent des renseignements scientifiques et techniques qui constituent une contribution aux connaissances actuelles, mais qui ne sont pas normalement appropriés pour la publication dans un journal scientifique. Les rapports techniques sont destinés essentiellement à un public international et ils sont distribués à cet échelon. II n'y a aucune restriction quant au sujet; de fait, la série reflète la vaste gamme des intérêts et des politiques de Pêches et Océans Canada, c'est-à-dire les sciences halieutiques et aquatiques.

Les rapports techniques peuvent être cités comme des publications à part entière. Le titre exact figure au-dessus du résumé de chaque rapport. Les rapports techniques sont résumés dans la base de données *Résumés des sciences aquatiques et halieutiques.*

Les rapports techniques sont produits à l'échelon régional, mais numérotés à l'échelon national. Les demandes de rapports seront satisfaites par l'établissement auteur dont le nom figure sur la couverture et la page du titre.

Les numéros 1 à 456 de cette série ont été publiés à titre de Rapports techniques de l'Office des recherches sur les pêcheries du Canada. Les numéros 457 à 714 sont parus à titre de Rapports techniques de la Direction générale de la recherche et du développement, Service des pêches et de la mer, ministère de l'Environnement. Les numéros 715 à 924 ont été publiés à titre de Rapports techniques du Service des pêches et de la mer, ministère des Pêches et de l'Environnement. Le nom actuel de la série a été établi lors de la parution du numéro 925.

Canadian Technical Report of
Fisheries and Aquatic Sciences 3237

2017

EXTRACTION OF VESSEL ACOUSTIC SOURCE LEVELS AND TOTAL SOUND EXPOSURE LEVELS FROM PASSIVE ACOUSTIC RECORDINGS ON THE EASTERN NOVA SCOTIAN SHELF SLOPE AND IN THE GULLY MARINE PROTECTED AREA

by

N.A. Cochrane and H.B. Moors-Murphy

Department of Fisheries & Oceans
Maritimes Region
Ocean and Ecosystem Sciences Division
Bedford Institute of Oceanography
PO Box 1006
Dartmouth, NS
B2Y 4A2

Cat. No. Fs97-6/3237E-PDF ISBN 978-0-660-23610-0 ISSN 1488-5379

Correct citation for this publication:

Cochrane, N.A. and Moors-Murphy, H.B. 2017. Extraction of vessel acoustic source levels and total sound exposure levels from passive acoustic recordings on the eastern Nova Scotian Shelf Slope and in the Gully Marine Protected Area. Can. Tech. Rep. Fish. Aquat. Sci. 3237: viii + 67 p.

TABLE OF CONTENTS

LIST OF FIGURES

ABSTRACT

Cochrane, N.A. and Moors-Murphy, H.B. 2017. Extraction of vessel acoustic source levels and total sound exposure levels from passive acoustic recordings on the eastern Nova Scotian Shelf Slope and in the Gully Marine Protected Area. Can. Tech. Rep. Fish. Aquat. Sci. 3237: viii + 67 p.

Vessel broadband acoustic source levels (SLs) and total passage sound expose levels (SELs) are computed and tabulated for 24 passages of commercial vessels proximate to three deep-moored (~1500 m) acoustic recorders on the outer Scotian Shelf/Slope. Required vessel trajectories were determined from exactEarth satellite AIS fixes while acoustic transmission loss estimates were obtained from a Parabolic Equation model with outputs simplified to empirical frequency-independent decibel forms with logarithmic slant range dependencies. Container vessels and bulk carriers displayed, on average, higher SLs than tankers and cargo ships, but no definitive correlations between near-broadside aspect vessel SLs and either vessel gross tonnage or vessel speed were evident. Vessel SLs in stern aspect appeared several dB higher than in bow aspect. Extracted source levels are compared to those from an independent published study in the Santa Barbara Channel.

RÉSUMÉ

Cochrane, N.A. and Moors-Murphy, H.B. 2017. Extraction des niveaux de source acoustique des navires et du total des niveaux d'exposition au bruit des enregistrements acoustiques passifs dans la partie est du plateau/talus néo-écossais et dans la zone de protection marine du Gully. Rapp. tech. can. sci. halieut. aquat. 3237: viii + 67 p.

Les niveaux de source acoustique à large bande provenant des navires et le total des niveaux d'exposition au bruit des passages sont calculés et compilés pour 24 passages de navires commerciaux à proximité de trois enregistreurs acoustiques ancrés profondément (1500 m) sur la zone externe du plateau/talus néo-écossais. Les trajectoires requises par les navires ont été déterminées à partir de correctifs du SIA satellite d'exactEarth, tandis que les estimations sur la perte de transmission acoustique ont été obtenues à partir d'un modèle d'équation parabolique avec résultats simplifiés sous forme de décibels sans dépendance fréquentielle avec dépendances logarithmiques à distance oblique. Les navires porte-conteneurs et les vraquiers affichent, en moyenne, des niveaux de source plus élevés que les pétroliers et navires de charge, mais il est impossible de tirer des corrélations entre les niveaux de source de proximité du navire et soit le tonnage brut du navire, soit la vitesse du navire. Les niveaux de source du navire près de la poupe semblaient de plusieurs dB plus élevés que près de l'étrave. Les niveaux sources extraits sont comparés à d'une étude indépendante dans le chenal de Santa Barbara.

1. INTRODUCTION

This report analyzes noise radiated from individual vessels as monitored at three deep water (~1500 m) sites off Nova Scotia. Data were recorded using JASCO **A**utonomous **M**ultichannel **A**coustic **R**ecorders (AMAR) in May and June 2013. Station "MidGul" was located in the Gully canyon while stations "GulSho" and "ShoHald" were located further east on the Scotian Slope between the Gully and Shortland Canyon and between Shortland and Haldimand canyons respectively (Table 1).

The present report is a companion document to Cochrane and Moors-Murphy (2017); the primary report explored the fundamental characteristics of the complete broadband passive acoustic dataset extending from September 2012 to September 2014 at the above three sites. In-depth treatment of recorded vessel noise was deemed to warrant a separate document. Particulars pertaining to station locations, mooring geometries, AMAR properties, and the detailed acoustic character of the datasets are provided in the primary report.

Vessel noise, which normally constitutes the main source of ocean acoustic noise in the roughly 10 Hz to 1 kHz range, possesses an extensive literature spanning many decades due to its military and, more recently, its environmental implications. For convenience we divide vessel noise into two broad categories: "Close range" vessel noise arises from discrete, usually easily identifiable sources in the vicinity of the acoustic detector. Its amplitude declines rapidly with vessel range until at a few 10's of km for non-directional detectors, such as our AMARs, it tends to disappear into a temporally/spatially relatively stable background continuum of "long range" vessel noise. The long range vessel noise component originates from the superposition of numerous, individually unidentifiable vessel sources at long distances from the detector. Because of the low innate acoustic absorption characteristics of the ocean below 1 kHz, significant long range vessel noise sources can be distributed over large portions of deep ocean basin such as the North Atlantic.

The objective of this study was to extract quantitative descriptors of radiated noise attributable to identifiable individual vessels and vessel types, from a collection of well delineated ship passages proximate to each of the moorings. This study also lays the groundwork for a relatively **simple** predictive model by which both the instantaneous and cumulative (i.e. time integrated) noise level generated from a known ship type can approximated with useful accuracy as a function of range, vessel aspect, speed and environmental factors although formal development of such a model was considered outside the scope of the present study.

The extraction of quantitative vessel-specific measures of radiated ship noise from remote measurements can be challenging. The ocean, including its upper and lower

boundaries, constitutes a complex propagation medium. Spatially and temporally (esp. seasonally) variant ocean temperature/salinity structures together with the effect of pressure define ocean sound speed distributions that refractively control the geometry of sound propagation paths. Frequency dependent acoustic absorption is largely controlled by the same temperature and salinity structures but with different dependencies than for sound speed. Spatially and temporally variable propagation boundary conditions occur at both the top and bottom of the water column, namely a variable roughness acoustic pressure release surface interface and an irregular, spatially variant acoustic impedance and sound speed mismatch at the bottom boundary which controls sound reflection/transmission properties from/into the seabed. In addition to propagation effects, noise from individual vessels at range is observed against a spatially and temporally variant ambient background with components both from long range ship noise and from natural highly variant wind/wave fields that can influence the discernment and quantification of individual vessel signals.

We proceed by first addressing the determination of vessel trajectories that define instantaneous source-receiver geometries. We then quantitatively model the acoustic transmission loss for representative geometries and propagation medium characteristics. Finally, these two information streams are used in concert to extract vessel-specific acoustic source characteristics from the relevant acoustic field data.

2. APPROACH

2.1. VESSEL TRACK DATA

2.1.1. Extraction of AIS Vessel Tracks

Quantification of the source characteristics of vessels of opportunity from AMAR acoustic recordings requires knowledge of the precise spatial/temporal geometry of the relevant vessel passage in relation to the acoustic receiver at range. Fortunately, most large vessels, fishing vessels excepted, are required to carry **A**utomatic **I**dentification **S**ystem (AIS) tracking beacons[1]. AIS beacon transmissions are monitored and recorded by strategically placed ground stations and, recently, orbiting AIS detection satellites. Since our AMAR mooring sites lie beyond the ~100 km range for reliable monitoring from shore-based ground stations, orbiting platforms supply the bulk of our off-shore vessel AIS data.

The Canadian company exactEarth furnished to DFO the raw satellite-relayed AIS data used in this 55 day study extending from 7 May to 30 June 2013. Study initiation coincided with the Summer 2013 AMAR mooring deployments (7 – 8 May), while the chosen duration restricted analysis to the initial two-month post-deployment interval.

[1] The International Maritime Organization's (IMO) International Convention for Safety of Life at Sea (SOLAS) regulations (V/19) require AIS beacons be placed on all international voyaging vessels ≥ 300 GT. Canadian law, in addition, requires AIS beacons on all domestic vessels ≥ 500 GT and on most passenger vessels. Fishing vessels are exempt.

The time constraint ensured that any temporal drifts in AMAR hydrophone sensitivity and possibly related anomalous increases in recorder internal noise levels observed late in at least some deployments, (Cochrane and Moors-Murphy 2017) would be minimal. Importantly, the chosen window kept analytical data volumes readily manageable while still adequate for a pilot study.

Custom in-house developed software was used to extract vessel identification, and positional parameters from standard AIS "!AIVDM" data packets while interspersed NEMA "$PGHP" strings provided corresponding time stamps. Definitions of AIS protocols and message types are available from a variety of online sources; Raymond (2014) providing especially comprehensive and detailed information with periodic updates. Our custom software routines decoded AIS message types 1, 2, 3, and 18 with file output in the form of successive ASCII text records with the following comma-delimited fields formatting:

Year (integer),
Month (integer),
Day (integer),
Hour (integer),
Min (integer),
Sec (fractional) - all time quantities derived from last-decoded $PGHP string),
Channel ("A" or "B"),
Vessel MMSI # (9-digit integer),
Vessel North Latitude (fractional degrees, negative for south lat),
Vessel East Longitude (fractional degrees, negative for west long),
Vessel Speed over Ground (fractional knots),
Vessel Course over Ground (fractional degrees),
Vessel Heading (fractional degrees)

Several data filtering options were integrated into our decoding tools, the most important being restriction of output data to vessels within a specified Lat – Long box, and further restriction of output data to vessels within a specified radius of a specified geographic point (flat earth geometric approximations are normally sufficiently accurate for radii < 100 km). The latter option, in operation, computed and appended vessel range and bearing from the specified point to the above output stream.

Also, in operation, quality control checks were performed for corrupted data records and for invalid or unreasonable data values. Suspect records were rejected. Occasionally, corrupt data evaded automatic detection but instances were infrequent.

Decoding tools were also developed for AIS type 5 messages consisting of 2-sentence strings that contained the vessel MMSI and IMO #'s, vessel call signs, vessel name, numeric ship type designation, and vessel physical dimensions. In reality, these additional decoding routines were of lesser value since type 5 messages were infrequently received compared to the shorter message types previous. However, they were useful for the construction of tables of detected vessels within defined time periods over relatively

wide geographic areas that could potentially be used to resolve the not infrequent ambiguities in vessel identification inherent with the shorter message types.

Identification of specific vessels using received MMSI #'s in isolation (using message types 1, 2, 3, and 18) was frequently problematic. Based on Internet searches, multiple vessels often appeared to possess the same MMSI #. In a few cases this was seemingly true, but in other instances merely apparent due to the retirement of one vessel and the subsequent release and reassignment of its MMSI # (in these cases vessel IMO #'s usually differed). Vessel ownership could also change often resulting in a change in vessel name, but retention of the original MMSI #. A vessel might also acquire a new AIS beacon with a new MMSI #. Similar problems also accompanied IMO #'s. If MMSI #'s in isolation were employed for vessel identification, ambiguities could often be resolved by reference to catalogued vessel itineraries and/or catalogued type 5 messages (above).

All eastern Scotian Shelf/Slope AIS-detected vessel positions for the 7 May – 30 June 2013 study period bounded by latitudes 43.0 to 45.0º N and longitudes 57.0 to 60.6 W are shown in Figs. 1 to 3. Figs. 1 and 2 show position data captured from class A only and class B only AIS transceivers respectively. Figure 3 shows the class A and class B transceiver position data combined and colour coded according the 6th digit (essentially random) of the respective vessel MMSI #. Colour coding allowed discernment of individual vessel tracks with fewer ambiguities using simple visual inspection. For example, note the evidence for at least two differing vessels participating in the localized intense (probably petroleum related) activity just south of Sable Island. The three AMAR mooring locations for the Summer 2013 deployments appear as black dots with enclosing circles (green) of 20 km radius. Inferred vessel tracks passing near the mooring locations tended to be straight over extended spatial intervals, as might be anticipated for most commercial shipping. Nevertheless, vessel fixes were often quite sparse resulting in frequent extended navigation gaps within individual inferred vessel transects, the 2013 constellation of AIS monitoring/relay satellites being insufficient to produce continuous temporal coverage of the area around our moorings. Consequently, in the absence of a concerted effort to interpolate the most discontinuous vessel tracks, only **lower** bounds could be confidently placed on the commercial marine traffic densities near each acoustic mooring.

Initially, the AIS database for the 55-day study period was searched for all vessel detections within 20 km radii of each acoustic mooring site. Next the non-ambiguous identities and basic descriptors of essentially all vessels entering the 20 km radii around each mooring site were established and tabulated by reference to catalogued vessel MMSI #'s and on-line vessel historic itineraries. Several instances of multiple passages by the same vessel within the study period were detected. The result of the search was:

- MidGul – 14 different vessels detected, 1 vessel making 2 passages, for a total of 15 passages or 0.273 passages/day.

- GulSho – 26 different vessels detected, 3 vessels making 2 passages and 1 vessel making 3 passages, for a total of 31 passages or 0.564 passages/day.

- ShoHald – 26 different vessels detected, 3 vessels making 2 passages, for a total of 29 passages or 0.527 passages/day.

From the above summary the marine traffic density over the study period near the two eastern stations, GulSho and ShoHald, appeared about double that for MidGul.

2.1.2. Estimation of Marine Traffic Densities

It is instructive to state the minimum inferred marine traffic density within the study radii around each station in more conventional units. Traffic density can be estimated from statistical arguments based solely on the above-derived passages/day rather than the more rigorous and accurate - but more time-consuming - extrapolation and detailed examination of all individual ship detections and tracks over wider areas of the Scotian Shelf. Assuming that ships transited the 20 km radius mooring circles **at random** (1st simplifying assumption) the **average** length of a single transit was:

$$L_{Transect} = 40\,km \times \tfrac{1}{2} \int_{-1}^{1} \sqrt{(1-x^2)}\,.dx = 40\ km \times \frac{\pi}{4} = 31.42\,km$$

Using the **average** speed v_{av} (estimated at about 13.9 knots or 7.15 m/s) of vessels passing through the three mooring areas combined, the average dwell time for a vessel incursion (a 2nd and more controversial simplification) was calculated to be 31.42 x 10^3 m / 7.15 m/s = 4.394 x 10^3 s (i.e. modestly in excess of 1 hour). Considering the case of MidGul, we observed an average of 0.273 ship passages/day or an average ship dwell time of 4.394 x 10^3 s/passage x 0.273 passages/day = 1.200 x 10^3 s/day. These dwell time seconds were designated as "ship seconds" as they were generally accumulated over multiple ships. Since the area enclosed by a 20 km radius is 1.2566 x 10^9 m^2, we restated the 1.200 x 10^3 ship s/day in terms of ship traffic density with units (ship s)/(s m^2):

1.200 x 10^3 ship s/day x (1 day / 86400 s) x (1 / 1.2566 x 10^9 m^2) =

1.105 x 10^{-11} ship s/(s m^2)

Formalizing the above reasoning and letting S_{pd} be the ship incursion rate into a circle of radius r:

$$\frac{Ship\ s}{s\ m^2} = \frac{S_{pd} \cdot \frac{\pi}{4} . 2r}{v_{av} .86400 .\pi r^2} = \frac{S_{pd}}{172800 .v_{av} .r}$$

On substitution of the appropriate numeric values for MidGul the above relation yields the identical result to the step-by-step calculation above. Corresponding values for

GulSho and ShoHald scale linearly with S_{pd} yielding 2.28 x 10^{-11} and 2.13 x 10^{-11} ship s/(s m^2), respectively.

The AIS-based estimates of mainly inshore ship traffic by Simard et al. (2014) used a "mean traffic density" stated in (*sic.*) "daily ship-hr km^{-2} ". This quantity appears similar to our own but expressed in differing units, seemingly:

$$\frac{Ship\ h}{Day\ km^2} = \frac{Ship\ s}{s\ m^2} \times \frac{86400\ s}{1\ day} \times \frac{1\ hr}{3600\ s} \times \frac{1 \times 10^6\ m^2}{1\ km^2} = 2.4 \times 10^7\ \frac{Ship\ s}{s\ m^2}$$

Using the above relationship the mean traffic density for MidGul above translates to 2.652 x 10^{-4} daily ship-hr km^{-2}.

These results should be interpreted cautiously as the crude approximations used for some variables represent an over-simplification of ship behaviour; perhaps most notably our use of average ship speed to compute dwell times for an ensemble of transect lengths. Actual commercial shipping speeds vary widely from about 9 to at least 20 kts, and therefore should not be arithmetically averaged prior to the computation of the inverse related dwell times. More importantly, the number of ship incursions is underestimated, perhaps by as much as 50%, as a consequence of the AIS drop-outs between successive satellite passes. Unless a vessel was directly detected within one of the 20 km radii it was not counted. Consequently, the incursion rates employed and **the resultant traffic density estimates should be regarded only as lower bounds**. The computations above might be expected to furnish modestly better than order-of-magnitude estimates to the true marine traffic densities. More tedious methodologies might recover some vessel passages characterized by sparser AIS coverage than those detected above and statistical arguments might be possible in regard to the fraction of vessel passages remaining undetected but this lies beyond the present project scope.

2.2. MODELLING ACOUSTIC TRANSMISSION LOSS

2.2.1. Acoustic Propagation Model and its Parameterization

Let us further consider the extraction of a given vessel's acoustic properties from a stationary moored AMAR recording. In general, vessel-emitted noise energy geometrically diverges or spreads from the source, is absorbed by the propagation medium, and is otherwise modified by its propagation path or paths and boundary reflections before impinging on the remotely situated receiver. Acoustic propagation from source to receiver is normally considered a linear process where the in-transit source-to-receiver signal modification expressed in the frequency domain can be characterized by a frequency dependent, but amplitude independent, transmission loss (TL). To infer vessel acoustic properties from remote measurements one must develop an appropriate propagation TL model incorporating an adequate representation of both the source–to-receiver geometry and the physical properties of the acoustic propagation medium including its boundary conditions. The properties of the medium are less critical and therefore more readily specified at shorter observation ranges where the complexity

of resultant source to receiver propagation paths is minimal. Shorter analysis ranges also better ensure that assumed vessel noise signals do originate largely from the vessel in question.

We model frequency domain acoustic TL using the 2-D Parabolic Equation (P.E.) technique (Jensen 2000); specifically, an in-house tailored version of the public domain P.E. "RAM" (**R**ange-dependent **A**coustic **M**odel) code of Collins (1993) refined to Version 1.5 downloaded (previously) from the ram.nrl.navy.mil website.[2] Essentially identical codes were previously employed at the Bedford Institute of Oceanography (BIO) to model TL for ocean bottom seismometer (OBS) hydrophone signals received from seismic exploration airgun sources during the 2003 Marathon Canada, Scotian Shelf/Slope exploration seismic survey (Cochrane 2007). Since all three Summer 2013 acoustic moorings were deployed in 1500 - 1600 m water depths (Table 1) with the omnidirectional AMAR hydrophones (Geospectrum M8E) suspended about 60 m above bottom, a single representative geometry was modelled consisting of a mooring in 1560 m total water column depth with the receiver hydrophone at 1500 m depth.

The earlier Marathon survey related studies (among others) showed that outer Scotian Shelf sound speed profiles varied significantly and systematically over the May – June time period. The water column upper 100 - 120 m in early spring was characterized by cold, low salinity Scotian Shelf waters of comparatively low computed sound speed. These colder waters persisted only at depth during the summer months in the form of a low sound speed channel centered at ~100 m depth as the cold layer was progressive capped during late spring/early summer by a warmer, higher sound speed layer building down from the surface with the growth of the seasonal thermocline. At still greater depths, sound speeds were subject to two competing influences, a general decline in sound speed with depth due to decreasing temperatures associated with the main (deep) ocean thermocline, and a general increase in sound speeds from increasing hydrostatic pressure. The pressure effect became increasingly dominant as depths approached 1000 m, which in the slope waters immediately adjacent to the Scotian Shelf usually resulted in a broad sound speed minimum in the 400 – 600 m depth range. This minimum constitutes the central axis of the so-called deep ocean sound channel, the depth of which varies systematically over the North Atlantic Basin (Urick 1975) being much deeper in the tropics than in more polar latitudes. The earlier study showed that acoustic energy propagating laterally to long ranges on the Scotian Shelf/Slope tended to become trapped around the axes of both, the shallow and deep sound channels, where the periodic, undulating refraction-controlled ray paths minimized lossey sound interactions with the water surface (at least in summer for the shallow sound channel) and with the ocean bottom.

Limited site and time-specific sound speed information existed for the summer 2013 study period. The most relevant sound speed profile was derived from a CCGS *HUDSON* Cruise 2013-008 Moving Vessel Profiler (MVP) sampling line which passed close to MidGul at 10:04 UTC on 23 May 2013 (specifically: Profile MVP_2013-05-23-070444.raw collected nominally at 43° 53.222' N 58° 55.679' W). The MVP

[2] A current FORTRAN code source is http://oalib.hlsresearch.com/PE/RAM/ram.f (26 June 2017).

temperature/salinity (TS) vs. depth profile defined the sound speed profile in the top 200 m. Sound speed structures from 200 m to bottom, below the sampling depth of the MVP, relied upon TS data from an historical 25 May 2003 *HUDSON* CTD profile: "2003May25_HUDSON_do21a008_based.txt" collected at 43° 51.39' N 58° 56.20' W. The combined TS profile and the resultant sound speed profile computed using the formulation of Mackenzie (1981) is shown in Fig. 4. In the absence of better site/time-specific data, this same oceanographic profile was used to model acoustic propagation to all three Summer 2013 AMAR receivers.

Acoustic parameterization of the seabed followed that of Cochrane (2007) with an effectively infinite depth sub-bottom of 1750 m/s compressional wave velocity, 0.7 dB/wavelength (λ) acoustic absorption, and 1.9 specific gravity (S.G). As in the 2007 study it was understood that 1 to 2 m of very fine grained sediment with acoustic properties nearly matching those of seawater commonly overlaid the harder substrate although the effects of any such surficial layer should be virtually immaterial for a hydrophone placed 60 m above the interface. Sub-bottom propagating shear waves were not considered in our current version of the RAM model.

Cursory examination of noise spectra from multiple ship transits within several kilometres of the three AMAR sites revealed that the geometric mean of the lowest spectral frequencies clearly of ship origin was about 20 Hz, while the geometric mean of the highest significant ship frequencies was just over 900 Hz. These facts suggested ship passages should be evaluated and modelled in the frequency range of roughly 20 Hz to 1 kHz (frequency ranges varied vessel-to-vessel). When acoustic spectral sections at high frequency and high temporal resolutions (i.e. sonogram sections) were examined for close ship passages, complex multi-path acoustic interference phenomena were usually observed at and around the times of closest passage. In P.E. modelling it was considered expedient to maintain sufficient grid resolution, both vertical and horizontal, and sufficiently high order RAM model Padé coefficients to reproduce such interference effects at any given **single** frequency. However, the numeric simulation of **elementary** vessel passage frequency x time sonogram interference patterns for a fixed mooring at short lateral observation ranges is most readily achieved by employing acoustic ray models (APPENDIX 1). This is because P.E. numeric models cannot guarantee the accurate modelling of energy reflecting off bottom at grazing angles exceeding approximately 70^0; nor is P.E. simulation an especially efficient modelling process for very closely spaced frequencies extending across wide frequency bands.[3]

We chose to model P.E. TL vs. range for 5 broad 1/3 octave wide bands (or bins) with center frequencies spanning the range 20 to 1000 Hz (bin boundaries were **not** intended to be contiguous in frequency). In strict geometric progression these bins would be centered at 20, 53.18, 141.4, 376.1, and 1000 Hz. In practice, the bins were approximated by substitute bins at the convenient rounded center frequencies of 20, 50, 150, 400, and 1000 Hz respectively. Within each 1/3 octave wide bin, 10 geometrically

[3] Due to the unusually high order Padé series utilized in our P.E. simulations (below), reflected ray phases are probably accurate to grazing angles considerably higher than 70º. The stated angular limit for validity should therefore be regarded as conservative.

spaced frequencies between the higher and lower band limits were utilized to P.E. model acoustic pressure squared. Pressure squared was averaged over the 10 constituent frequencies to define a 1/3 octave average squared pressure, from which the vessel source to AMAR receiver numeric TL (in decibels) was computed. The primary reason for averaging over a specific band(s) of closely spaced frequencies in the case of broadband ship noise was to obtain a TL(s) characterizing the bin central frequency(s) that was significantly less spatially variant (i.e. of a less local character) due to acoustic multi-path interference effects than would otherwise characterize a strictly monochromatic P.E. solution(s) at the bin central frequency(s).

2.2.2. Description of Propagation Modelling Results

P.E. computed TLs from a vessel source to a hydrophone receiver at a depth of 1500 m were extracted for source to receiver lateral ranges up to 20 km utilizing 20 km horizontal x 2500 m vertical dimension simulation grids. Computations for 1/3 octave frequency bins with center frequencies of 20, 50, and 150 Hz utilized horizontal x vertical grids of 6000 x 8192 pts and retained 10 Padé coefficients. Similar computations for 400 and 1000 Hz center frequencies utilized grids of 12000 x 16384 pts and retained 13 Padé coefficients. Computations at all frequencies utilized the "self starter" point source (Collins 1992), as packaged with RAM Version 1.5, placed at 0 m lateral range and 10 m depth, the assumed vessel average propeller depth. An artificial strong acoustic absorbing layer was placed sub-bottom beginning 1800 m from the surface and extending to the 2500 m bottom grid boundary to effectively eliminate spurious acoustic reflections off the same. Illustrative P.E. computed, colour-coded sound pressure level sections at **single** frequencies (frequency averaging not employed) of 50 and 1000 Hz are shown in Figs. 5 and 6 respectively.

For plotted pressure levels a cylindrical spreading 10 log (lateral range) decibel dependency was removed to minimize the total pressure dynamic range for increased clarity in delineating details of the propagation processes. Graphical curves of decibel TL from the source at 10 m depth to the AMAR receiver at 1500 m depth, 60 m above ocean bottom, vs. lateral range from the source have been overlaid in white (Figs 5 and 6). These curves, in contrast to the colour-coded data of the background plot, show actual numeric total TL without the removal of any cylindrical spreading loss component. Since the plots are for single frequencies without frequency averaging, detailed acoustic interference effects arising from sea surface and bottom reflections are strong and clearly discerned especially at 50 Hz (Figs 5 and 6). At 1000 Hz, much of the detailed phasing effects occur at spatial frequencies not properly resolved at the limited pixel resolution of the reproduced figure.

Resultant TL vs. horizontal lateral range, computed and averaged over the 1/3 octave width of each of the 5 frequency bins (as explained in Section 2.2.1) are shown in Fig. 7. On making allowance for residual multi-path interference effects persisting even after wide band averaging, a simple and roughly consistent TL range dependency is observed to emerge for, particularly, the four higher bin frequencies while the 20 Hz results diverge somewhat from this pattern at longer ranges. The divergence of the 20 Hz bin

results might be largely attributable to the proximate pressure release water surface only 10 m above the source, a distance corresponding to only about 14% of the acoustic wavelength at the bin center frequency. From the alternative perspective of simple acoustic ray theory, the 20 Hz source pressure signal will be largely cancelled by its phase inverted surface-reflected image over all radiation angles.

2.3. EXTRACTION OF VESSEL ACOUSTIC NOISE CHARACTERISTICS – PRACTICAL CONSIDERATIONS

2.3.1. Extraction of Vessel Broadband Acoustic Source Levels

Vessel noise levels have traditionally been measured at close ranges in a small number of dedicated facilities that allow precise determination of spectral domain source radiation patterns as functions of observation azimuth and dip angle, and vessel speed. Such detailed characterizations of a given vessel are often difficult, if not impossible, to obtain. A simpler characterization, often used for environmental assessment purposes, is to quantify vessel noise in terms of a single numeric broadband RMS source level (SL) occasionally with very limited attention as to how this parameter might vary with vessel speed or observation aspect (for instance, broadside vs. bow or stern aspect). In our case, given the AMAR-derived spectral signature of a passing vessel and the corresponding AIS-derived vessel trajectory, it should be possible to derive the broadband vessel-specific acoustic source level with the use of an applicable TL model. Since the AIS vessel identity is also known, derived source levels can be compared to those measured elsewhere for similar classes of vessels. Reasonable agreement would constitute a validity check on our TL modelling and also lend confidence to our ability to predictively model, if required, the spatial/temporal noise impacts of hypothetical vessel encounters.

Consider the time domain variance of the vessel source pressure level, P_S, over a specific time interval. The variance can be written as a band-limited integral of the source pressure spectral density for the same time interval:

$$\text{var}\, P_S = P_{S\,RMS}^2 = \int_{f_1}^{f_2} S_S(f)\, df$$

Frequency limits f_1 and f_2 define the range over which the source radiates significant acoustic energy.

The variance of the received pressure level, P_R, can be similarly written in terms of the observed band-limited received acoustic pressure spectral density:

$$\text{var}\, P_R = P_{R\,RMS}^2 = \int_{f_1}^{f_2} S_R(f)\, df$$

Consider the case of a frequency dependent TL applied to an acoustic source spectral pressure signal (defined by the pressure spectral level measured at a reference distance of 1 m) to characterize propagation to a remotely situated acoustic receiver:

$$S_S(f) = S_R(f).\,TL_{SRL}(f)$$

TL has been expressed as a linear multiplicative factor (> 1) rather than its common decibel form (if decibel TL is defined as a positive signed quantity this linear form is dictated).

Consequently, given a both a vessel's received noise spectrum within a defined time window and the applicable model-derived, frequency dependant TL, the vessel source spectral level can be computed from the immediately preceding relationship. In turn the variance of the vessel source sound pressure level can be obtained by frequency domain spectral integration:

$$P^2_{S\,RMS} = \int_{f_1}^{f_2} S_R(f).\,TL_{SRL}(f)\;df$$

Practical evaluation is much facilitated if TL_{SRL} (f) can be **assumed** frequency independent. In such instances the above simplifies to:

$$P^2_{S\,RMS} = TL_{SRL} \int_{f_1}^{f_2} S_R(f).\,df$$

Reverting to conventional decibel notation by taking 10 log of both sides of the equation; defining the acoustic source level, *SL*, as 20 log ($P_{S\,RMS}$); and approximating the integral by a real-world finite resolution spectral summation:

$$SL_{dB\,RMS} = TL_{SR\,dB} + 10.0\,\log\left(\sum_{f_1}^{f_2} S_R(f)\,.\,\Delta f\right) = TL_{SR\,dB} + SPL_{dB\,RMS}$$

The last relation constitutes a broadband form of the conventional sonar equation with TL defined as a +ve quantity. The last term represents the received decibel sound pressure level, *SPL*, following the terminology of Clay and Medwin (1977).

For the case of a near-surface source and a remote receiver, the TL range dependency can be stated in terms of either slant or lateral range. TL is a lumped measure of many processes including source patterns, signal spreading, refraction (including trapping within vertical sound channels), boundary reflections, and absorption within both the ocean (~ 1 dB at 1000 Hz for a 20 km path), some, if not most of these processes being inherently frequency dependent. In actual practice, however, an overall roughly logarithmic functional form for lumped decibel TL vs. source-to-receiver range has been frequently reported. This is most clearly observed if the measured signals are reasonably broadband so as to reduce the extreme multi-path phasing effects characteristic of monochromatic signals. Often the TL is observed to closely approximate a 20 log (range) dependency. While geometric ray theory would indicate a near 20 log (range) spherical spreading dependence should be observed only very close to a point sound source where the comparatively weaker reflections from bounding water column interfaces can safely be ignored, in practice it has often proven to remain a surprisingly

accurate empirical predictor of the smoothed TL at considerably longer ranges where a variety of additional loss mechanisms come into play (Urick 1975). Energy conservation, would suggest that TL at long ranges in a non-absorbing medium with lossless reflecting boundaries should be characterized by a 10 log (range) cylindrical spreading dependency. This cylindrical spreading assumption has sometimes been used in the absence of better theoretical or experimental controls to roughly estimate TL for all ranges from an acoustic point sound source exceeding the water depth - often by assuming 20 log R spherical spreading to a lateral range equal to the water depth followed by a smoothed transition 10 log (R/water depth) cylindrical spreading for ranges beyond. For real environments this approach may, in practice, differ little from, or even be less accurate than, the assumption of an invariant logarithmic fall-off applicable to all ranges. For example, Bassett (2010) observed a near-spherical 19.6 log (range) dependence for broadband ferry boat noise out to ranges of about 6 km in Puget Sound, ranges which far exceeded the prevailing water depth.

To investigate the case for our AMAR stations, the P.E. model derived TL data of Fig. 7 was re-plotted as a function of logarithmic **slant** range in Fig. 8. A roughly linear dependence of decibel TL on logarithmic slant range is observed, and as noted earlier that dependency is relatively independent of frequency, especially above 20 Hz. The best frequency independent fit overall was judged (by eye) to be:

TL_{dB} = 15.5 log (*Slant Range m*) + 10.8 dB

A fitting line based on the above relationship has been superimposed (solid black) on Fig. 8. Alternative spreading loss lines were also estimated and plotted in Fig. 8 of the form:

TL_{dB} = 10.0 log (*Slant Range m*) + 28.27 dB (cylindrical spreading at long ranges, plotted in black dotted)

TL_{dB} = 20.0 log (*Slant Range m*) - 3.5 dB (spherical spreading, plotted in yellow)

The latter two fits to the P.E. derived TL were seemingly poorer overall, especially the 10.0 log cylindrical-like fit.

The identical fitting lines were also plotted on Fig. 7 where the required slant range was derived from the displayed horizontal axis lateral range.

We chose the 15.5 log (Slant Range) line and the matching numeric relationship above as our primary working broadband TL regression with an assumed validity to ranges of at least 20 km. In Fig. 7, the 0 m lateral range (i.e. 1490 m slant range) intercept was assumed to be 60.0 dB. This TL was less than the 63.46 dB predicted by 20 log R spherical spreading contribution in isolation from source to receiver since under actual steady state conditions additional energy contributions at the receiver occur from both the vertically incidence water surface and the sea bottom interface reflections and their higher order reverberations. From a strictly energetic viewpoint, a close to 60 dB TL

appeared reasonable at 0 m **lateral** range: If the vessel is assumed represented by a high frequency, band-limited white noise point source at 10 m depth, the direct source-to-receiver ray, as above, will experience a 63.46 dB TL. Energy from a perfectly reflective surface should, on average, almost double the energy at the receiver, while energy contributed by the direct ray reflected off bottom will be scaled by the bottom reflection coefficient squared (0.38^2 by our parameterization), and similarly for the water surface reflected ray subsequently reflected off bottom on route to the receiver. Adding only these four energy contributions, each scaled by total path length spherical spreading and bottom reflectivity while ignoring higher order multiple reflections and any phase correlation effects, results in a combined TL of almost exactly 60 dB. While constituting less than a rigorous computation, this ray model based argument demonstrates that the model-fitting regressions were not unreasonable at short lateral ranges - the direct P.E. model solutions become unreliable at very high grazing angles (i.e. at short lateral ranges).

Observe that the P.E. TL simulation did not quickly tend to 10 log R cylindrical spreading at range, although beyond 10 km the slopes of all three lines were sufficiently similar that the optimal dependence with range was difficult to judge. In the modelled case, much energy emitted close to the horizontal appeared trapped in the surface sound channel (observed especially in Fig. 6) with little source energy reaching the near bottom region by direct ray paths (an acoustic shadow zone) for lateral ranges exceeding 10 km. Less obvious was the more subtle influence of the deep sound channel, broadly centered at around 550 m depth, which also exerted a slight upward refractive effect on sound otherwise radiated toward the bottom at very long ranges.

The P.E. modelling results do challenge or, at the very least, present a viable alternative to modelling practices that assume vessel (or airgun) noise must attenuate at a constant 10 log R cylindrical spreading rate at lateral ranges modestly exceeding the water column depth. For the considered case, a near 15 log R dependence seems preferable out to ranges of at least 10 water column depths. It will be remembered that for the lowest frequencies considered all three proposed curves, and the 10.0 log (R) curve in particular, constituted a systematic TL under-correction (i.e. TL is to a degree frequency dependent). The evident TL mismatch at low frequencies is probably not a major consideration since the bulk of vessel radiated noise tends to be confined to frequencies > 40 Hz.

In spite of the limitations (among others) of assuming a frequency independent TL, we believe that the simple TL relationships proposed above are sufficiently accurate for the purposes of this initial pilot study. Very importantly, they inherently possess the simplicity required for applicability to a considerable volume of field data within the resource constraints of the current project.

2.3.2. Estimation of Vessel Passage Sound Exposure Levels (SELs)

If broadband TL can be *reasonably* approximated by simple logarithmic range dependencies independent of frequency over a vessel's principal radiated noise band then computation of **theoretical** ship passage sound exposure levels (SELs) reduces to a

straightforward exercise. Proceeding along these lines, one can readily explore the theoretical fraction of total sound exposure accumulated within a given time of closest passage or, equivalently, within a given vessel range from the moored AMAR receiver. However, two major simplifications have been employed: a) Source levels of real vessels vary significantly with viewing aspect – which we do not consider; and b) real water depths vary with range and are undoubtedly important in characterizing actual TL and resultant received sound levels during extended vessel transects – which we also do not consider. Ignoring these complicating issues, theoretical cumulative ship passage SEL formulations are derived in APPENDIX 2 and their relevance and limitations further discussed in Section 3.1.2.

2.3.3. Time Base Considerations

For large commercial vessels travelling essentially straight line courses at constant speed, linear interpolation between several appropriately selected AIS time/spatial fixes can quite accurately and, for most practical purposes, adequately define their respective trajectories relative to a stationary acoustic mooring. However, precisely relating vessel location to the simultaneously recorded acoustic signal, particularly when a specific vessel is at short range from the receiver, requires that any offsets between the AIS and AMAR acoustic time bases be understood and compensated (vessel-to-mooring acoustic propagation times can usually be safely ignored). The low power consumption AMAR internal clocks can drift significantly relative to true time (believed essentially identical to AIS time) over the course of a deployment.

We attempted to circumvent effects from possible AMAR clock drift by establishing precise times for closest vessel approach within the AMAR acoustics time base itself using a purely acoustic-based methodology. AMAR acoustic data near the AIS times of closest ship passage were examined in the form of high spectral and high time resolution sonograms so that any interference fringes between vessel noise travelling by a direct path and by alternative one-hop surface and bottom reflection paths could be discerned. Individual interference fringes should minimize in spectral frequency at the AMAR times of closest vessel approach. Comparison of AMAR and AIS times of closest approach yield, in principle, the offsets between the two time-bases. This interferometric technique is detailed in APPENDIX 1.

3. RESULTS AND DISCUSSION

3.1. VESSEL NOISE CHARACTERISTICS – EXAMPLE 1

3.1.1. Vessel Source Levels

Can meaningful vessel acoustic source levels be extracted from our AMAR recorded data using the proposed frequency independent TL regression relations? Consider one

example: *VESSEL "M"*[4]; a 157098 GWT, 322 x 60 m tanker travelling at an AIS computed speed of 11.91 kts and on a course of 314º; passed to the NE of and within about 2.7 km of the surface projection of the GulSho mooring on 23 June 2013 at 04:25:14 UTC AMAR time (DOY 173.18194) as determined by sonogram-based interferometry (Fig. 9)[5]. A much lower resolution AMAR 1/3 octave time x log frequency spectrogram of the vessel passage is shown in Fig. 10 where normal calibration and frequency response corrections appropriate to the specific AMAR system (Cochrane and Moors-Murphy 2017) have been applied. The plotted power spectral noise estimates were extracted every 60 s (each estimate from underlying 20 x 32,768 pt non-overlapping time series sampled at 16 kHz) with 120 s data gaps occurring every 15 min when the AMAR was engaged in higher frequency sampling. In Fig. 10 it is noted:

1) The spectral signature of the vessel is clearly discerned at frequencies above 10 – 15 Hz. Higher spectral levels occasionally observed below 10 Hz are less clearly correlated with ship passage.

2) Spectral evidence of the ship passage extends to frequencies as high as several kHz. Maximum spectral levels at ≥ 1 kHz occur virtually simultaneous with closest vessel approach with significant spectral energy > 1 kHz confined to a relatively short time window symmetric about the time of closest approach. Little evidence for discrete spectral lines at > 100 Hz exists with the employed 1/3 octave frequency domain smoothing.

3) Spectral intensities peak in the 25 – 100 Hz range with strong evidence of several dominant spectral lines ≤ 100 Hz persisting even with the 1/3 octave smoothing. Vessel noise in the 25 – 100 Hz range dominates ambient background for the order of one hour either side of closest approach, but in an asymmetric manner - highest spectral levels are observed roughly 10 min **after** closest passage. A strong diagonally oriented, highly range dependent feature is present in the departure segment from about nearest passage to about 15 min post-passage. This feature would appear inconsistent with the simplest surface or bottom signal multi-path interference models. Otherwise, no obvious multi-path interference features are visible with the degree of frequency domain smoothing employed.

The spectral section of Fig. 10 is re-assembled in Fig. 11 together with plots of: 1) Computed broadband vessel source level; 2) vessel lateral range; and, 3) vessel aspect (horizontal plane). All four plots share a common time base. To derive broadband vessel

[4] In the public version of this report specific vessels are denoted by alphabetic letter to respect vessel and operator privacy on casual reading.

[5] Time stamps for acoustic data use the AMAR time base. Times of closest vessel approach are determined from the acoustic data using sonogram fringe observations and in this instance are believed accurate to ±60s AMAR time (estimated accuracy of determining time fringe minimum in isolation excluding other sources of systematic error). Vessel range at closest approach and average vessel speed over ground are determined from multiple AIS fixes. Vessel range as a function of AMAR time is computed using the AMAR time of closest passage, vessel lateral range at the closest geometric approach of the AIS trajectory, and AIS speed over ground. In this way the effect of any offsets between AMAR and AIS time bases in the matching of spectral times to vessel ranges is minimized.

acoustic source levels, decibel RMS received sound pressure levels were computed by first (linearly) multiplying 1/3 octave bin-averaged spectral levels by the associated frequency bin widths and then summing the results over all 1/3 octave bins covering the relevant frequency range, followed by decibel conversion.[6] Considering the original binning for the 1/3 octave estimates, the total effective frequency range integrated was 22.4 Hz to 905 Hz, a reasonable approximation to the nominal 20 – 1000 Hz range. Extracting broadband received sound pressure levels by spectral summation implicitly corrects the same for the frequency response of the measurement instrument and also band-limits the result, highly desirable effects not easily achieved by directly computing RMS levels from the time domain data. Band-limited, decibel RMS received sound pressure levels were converted to vessel RMS source levels by employing the logarithmic slant range TL formulae in Section 2.2.3, assuming 10, 15.5, and 20 log (Slant Range) dependencies.

In Fig. 11, the noted asymmetry in spectral levels about the point of closest approach is clearly reflected in the resultant vessel source levels: Source levels at near stern aspect appear ~ 7 to 10 dB higher than those near bow aspect. This result is consistent with other similar studies (McKenna et al. 2012). In this instance the asymmetry might also reflect the effect of rapidly decreasing water depths along the upslope transect unaccounted for in the present TL modelling. To draw valid conclusions regarding changing vessel aspect, the relevant analysed data must be limited to times when individual vessel noise clearly dominates ambient background (including distant shipping noise). Background noise is probably best approximated by the spectral levels near the left-hand (LH) plot boundary. In the current example, the nominal rise in computed vessel source levels observed on travelling backwards in time from about day 173.165 to the plot initiation is likely the spurious result of logarithmically increasing TLs being applied to a nearly invariant mostly ambient background noise component. The very broad peak in vessel source levels around DOY 173.19, most pronounced with application of the 10.0 and 15.5 log R corrections, might arise, at least partly, from the reinforcing effect of an in-phase bottom reflection combining with direct radiated propeller noise around the approximately 70 Hz maximum in the vessel's smoothed radiated noise spectrum. More likely, it constitutes a real feature in the vessel's (asymmetric) noise radiation pattern. The peak maximizes at an observation angle of about 30^0 off stern aspect. On proceeding to greater observation ranges, the vessel's aspect becomes increasingly astern, an angular aspect zone within which higher frequency radiated noise of many vessels has been observed to decrease, possibly a consequence of increasing wake absorption (Urick 1975; Arveson and Vendittis 2000). The essential absence of a broad symmetric peak prior to closest approach, i.e. with the vessel observed in corresponding bow aspect, is interesting and might argue for any bottom reflection interference effects being fairly minor. At longer ranges in departure aspect the 20 log R computed source levels tend to maintain a more consistent source level than the 15.5 log R levels, the 10 log R computed levels being even less consistent. This observation might suggest a superior realism for the 20 log R based TL curves when

[6] Considering the methodology by which the 1/3 octave binned spectral estimates were originally generated this summation is essentially identical to integration of the original high frequency resolution spectra over the equivalent frequency range.

applied to real field data. However, this conclusion is not definitive since, as noted, actual vessel source levels frequently decline at near stern aspect and the studied vessel was also travelling perpendicular to the bathymetric contours into rapidly declining water depths on the departure leg. Water depths decreased to about 600 m about 10 km past closest approach and to only about 130 m at 20 km beyond closest approach. A similar analysis of **approach** aspect source levels was hindered by vessel noise levels being closer to ambient background. Water depths on the approach leg were also deeper than those nominally modelled for TL, about 2200 m at 10 km prior to closest approach.

Source levels inferred at broadside aspect are probably the most reliable since they are inferred around nearest approach, often at lateral ranges of several km or less (see Section 3.2) where:

1) Numeric discrepancies between alternative TL formulations are minimized

2) Water depths still constitute reasonable approximations to the nominal depths modelled

3) Vessel origin noise levels are sufficiently high that little effect from the ambient noise background or fluctuations in the same is expected.

If we reject the 10 log (R) TL-based source level curve as the least likely to be realistic at short ranges, the two remaining curves furnish source levels in the range of 180 - 184 dB re 1 μPa^2 @ 1 m RMS. Source levels of this magnitude are not atypical of large vessels travelling at comparable speeds as analysed by McKenna et al. (2012), and, in fact, constitute a very good match to (McKenna's) oil tankers in isolation.

In Fig. 12, an attempt is made to improve upon the source level accuracies of Fig. 11 by an alternative processing technique that first subtracts the inferred ambient noise background, including the distant shipping background and any mooring-generated pseudo noise[7] from the utilized time domain spectral estimates. Ambient background was estimated by averaging the first 10 sets of spectral estimates starting at the LH side of the time domain spectral section in Fig. 11, assuming these earliest estimates to be totally uncontaminated by noise from the considered vessel. Comparing Figs. 11 and 12 it is observed that the broadside aspect source levels and the difference between approach and departure source levels observed at shorter ranges remain about the same – which is expected since these quantities were determined at relatively high vessel-to-ambient background noise ratios. The largest differences are observed for approach leg source levels at longer ranges where employed vessel noise levels were comparatively much reduced by subtraction of the assumed ambient (Fig. 12). Clearly, the effectiveness of this procedure is critically dependent on obtaining a representative and uncontaminated sample of ambient background and for the actual ambient background to remain stationary during the entire observation period (or at least while the observed vessel noise

[7] Mooring generated pseudo noise is not normally considered a component of true ambient background but the employed noise cancellation technique automatically effects its removal provided pseudo noise levels are temporally stationary.

signal is low). It does appear that real benefits often accrue from the subtractive procedure: Visually, vessel transits were more obvious on the spectral sections and less subjectivity was required by the analyst on deciding whether the vessel noise was sufficiently dominant at any given transect point to draw robust conclusions regarding source levels. This was especially true if plots generated with and without using subtraction could be compared.

Many uncertainties surround these vessel source level determinations, several already alluded to. Uncertainties in the exact acoustic nature of the bottom, and exclusion of modelled TL effects from sloping bottoms and rapidly changing water depths along profile water depths constitute two major sources of error. Additionally, the model-assumed TLs at 0 m lateral range could be several dB too high if, in reality, water surface reflections and perhaps some direct propeller radiation are attenuated by the vessel hull and/or vessel wake. Wake absorption effects are suggested by the asymmetry in low frequency vessel noise about closest approach. Might the absence of similar asymmetries at multi-kHz frequencies signify that the origin of much of the higher frequency sound is bubble collapse within the propeller wake itself somewhat spatially removed from the hull? What happens to modelled TLs if the vessel propeller is significantly deeper or shallower than the single modelled 10 m depth? Also the empirical TL formulations utilized are frequency independent, highly smoothed approximations to the P.E. model for a range-independent bathymetry. One might legitimately question whether the smoothing is excessive for some structures clearly seem in the P.E. model. These limitations should be kept in mind as we proceed to further detailed examples and general analyses.

3.1.2. Vessel SELs

In regard to the *VESSEL "M"* passage of the GulSho mooring; **theoretical** cumulative SELs (APPENDIX 2) were computed by numerical integration using 5 s time steps within expanding time windows out to 20,000 s on either side of mooring passage using the minimum range at passage, AIS navigation derived ship speeds, and the earlier estimated **broadside** vessel source levels. Both the theoretical cumulative SEL vs. time measured from closest passage and the same vs. Maximum (lateral) vessel range are plotted in Fig. 13. In each case, separate curves are shown for assumed 10, 15.5, and 20 log (slant range) based TL regressions. The single-value vessel source levels required for the computation were extracted from Fig. 11 at broadside aspect **specific to the TL regression relations employed** (180, 182, and 183.5 dB re 1 uPa^2 @ 1m for the 10 log, 15.5 log, and 20 log regressions respectively). This self-consistency procedure ensured essentially identical cumulative SEL contributions originating from the transect portion near closest passage so that the effects of differing TL formulations at longer computation ranges could be more clearly discerned. Note that no attempt was made to include vessel aspect effects in the employed source levels and TL's, and, as a consequence, in the resultant theoretical SELs.

In Fig. 13, it is observed that the theoretical cumulative SELs at long elapsed times continue to rise at a nearly constant rate when using the 10 log R TL formulation but, in

contrast, tend to level-off using the 15.5 log R and 20 log R dependencies. This observation is consistent with the SEL integral being undefined as $t_p \rightarrow \infty$ for a 10 log R based TL but remaining finite for the other two dependencies as discussed in APPENDIX 2. There is little difference between cumulative SELs out to accumulation times of at least 1000 s or about 6 – 7 km vessel lateral ranges regardless of the TL formulation employed, provided that the identical TL formulation has been used in the initial derivation of vessel source level.

Vessel SELs computed as above are **theoretical** constructs based upon general acoustic TL properties roughly consistent with predictions of the P.E. for an idealized representative geometry. Our theoretical SEL curves computed using TLs derived for constant water depth propagation paths (i.e. assumption of a smooth and level ocean bottom) should probably not be compared too critically to experimentally observed SELs (i.e. SELs computed from direct integration of received sound levels over time) except possibly for transect segments in the immediate vicinity of closest approach. Water depths frequently varied markedly and systematically along extended vessel tracks in our mooring areas. In computing these SEL curves the sole link to vessel-specific properties was the assignment of an aspect-independent vessel source level, even though significant aspect dependence is commonly observed for real-world vessels. Nevertheless, the theoretically computed SELs, especially their behaviours within extended time/range observation windows, could potentially capture important characteristics not easily explored by real-world measurement, for instance:

- In what manner would TLs and resultant SELs change if one were to replace late spring – early summer sound speed structures with those characteristic of late summer or winter?
- How would these same quantities change if the acoustic receiver were placed closer to the axes of either the shallow or deep sound channels?
- How would the same quantities be affected if vessel drafts deviate from 10 m?
- How would SELs change out to various ranges change if we introduced frequency dependent transmission loss?

For reference, experimental SELs for the above-considered ship passage are shown in Fig. 14. The computation consisted of a numerical frequency and time integration of the experimentally obtained 1/3 octave spectra employing the identical frequency sub-range selection, and ambient noise estimation and subtraction procedures utilized in the computation of the range and time dependent vessel source levels above. The entire vessel passage experimental SEL is defined as that accumulated over 4237 s before to 3683 s after closest passage. It computes to almost exactly 150 dB re 1 μPa^2 s. On comparison to the more theoretically derived SEL curves of Fig. 13, the experimentally computed value falls close to the 15.5 log R derived SEL curve for about 4000 s elapsed time both sides of closest passage. The same case theoretical SEL using the 20 log R based TL curve differs only slightly from that using the 15.5 log R curve.

The ambient noise subtraction process constitutes a potential source of bias in determining experimental SELs: The working assumption is that spectral noise levels observed at the start of analysis, approximately 4000 s prior to closest passage, sample a

pure and stationary ambient background, whose levels can be subtracted from all subsequently measured noise levels to yield ship-specific noise in isolation. On inspection, vessel noise levels in approach aspect tend to be significantly lower than those in departure aspect at equivalent ranges. Noise levels about 4000 s prior to passage appear to contain little same-vessel noise judging from spectrogram appearance. In contrast, noise levels nearing 4000 s post-departure (approaching the ends of analysed vessel transects), are often comparatively elevated, demonstrating that same-vessel noise components persist to longer ranges when the vessels are observed close to stern aspect. Consequently, the noise subtraction methodology probably does not greatly skew experimental total passage SELs - at least for the particular case considered - as the departure leg tends to be the major noise contributor at longer ranges. Nevertheless, subtraction will almost certainly result in some legitimate vessel noise being excluded from total passage SELs in consequence potentially biasing **experimental** SELs towards the lower slope15.5 log R and 20 log R TL **theoretical** SEL curves. Any attempts to improve significantly upon the present methodology by employing more time-removed and, consequently, less vessel-contaminated estimates of ambient background risk being counterproductive since ambient background does fluctuate on multi-hourly time scales from wind, intermediate range shipping, and mooring self noise contributions.

Of likely greater significance are the limitations of the current **theoretical** cumulative SEL models to account for real variations in source level with vessel aspect and for the changes in TL due to varying bathymetry associated with the continuously shifting transmission paths. In the above explored instance the approximate agreement between long transect cumulative SELs computed directly from experimental observations and those computed more theoretically by combining experimental vessel SL and simple frequency independent TL vs. log range type regressions is encouraging. With further verification over a wider database, the outlined theoretical approach could, as previously stated, prove useful for estimating cumulative SELs, in real or hypothetical situations where field data is limited or lacking. Contrasting geometries or medium properties would require reformulation of the TL vs. range regressions.

3.2. VESSEL NOISE CHARACTERISTICS – EXAMPLE 2

Do the simple SL extraction and theoretical cumulative SEL modelling techniques perform better if vessel transects run approximately parallel to, rather than perpendicular to, the general bathymetry (i.e. maintain near constant water depths along transect as assumed in derivation of the specific TL regressions above)? The comparatively smaller oil tanker *VESSEL "H"* (MMSI # xxxxxxxxx, 54800 GWT, 233 x 42m) on 25 June 2013 passed 1.720 km NW of GulSho on a course of 43^0 and speed of 11.04 kts. An identical series of analyses were performed (Figs. 15 - 19).

Again, a nominal 20 – 1000 Hz frequency range was examined although some vessel noise is discernable to several kHz (Fig. 15). Significant noise bursts are observed below 20 Hz, but not all bursts are clearly related to the vessel passage. While *VESSEL "H"* travelled slightly slower than the *VESSEL "M"* (11.0 vs. 11.9 kts respectively), *VESSEL "H"* passed closer to the acoustic mooring resulting in a more rapid transition from near-

bow to near-stern aspect (compare Fig. 16 vs. Fig. 11). Again, source levels derived near-stern aspect (in departure) exceed those in near-bow aspect (in approach), the difference for *VESSEL "H"* being about 4 dB vs. ≥7 dB for the previous vessel - assuming that these levels are reliably discernible at the extended ranges necessary to approximate near-stern and near-bow aspects. Some highly smoothed interference-like fringes are evident from 150 – 600 Hz on the low-resolution spectral section (Fig. 15) confined to the departure leg from day 175.775 to day 175.789. Informed by the ray-model interference plots of Appendix 1, these fringes might arise from bottom reflected energy even though the attendant 6 - 13 km vessel ranges are long for interpretations that ignore refraction. A brief spike in computed vessel source levels occurs at the point of closest approach (Figs. 16 and 17). While the spike's origin is uncertain, the underlying effect is clearly observed in the spectral levels in the ~ 25 – 200 Hz range. Might the extended tanker hull be excited as an in-phase line radiator giving rise to a narrow broadside radiation lobe? We have ignored the spike in interpolating the source level curves through closest approach. Broadside source levels for *VESSEL "H"* using the 10, 15.5, and 20 log R TL regressions were estimated, somewhat subjectively, as 184, 185, and 186 dB re 1 μPa^2 @ 1 m respectively; about 3 dB higher than those for the larger *VESSEL "M"*. Experimental total vessel passage SELs for *VESSEL "H"* were also approximately 3 dB higher (Fig. 19 vs. Fig. 14), the present experimental SELs agreeing slightly better with the 20 log R TL - derived theoretical SEL curves (Fig. 18). However, the 15.5 log R and 20 log R TL - derived theoretical SEL curves differed by only ~ 1 dB over for the cumulative time interval extending to 4000 s on both sides of closest passage.

3.3. VESSEL NOISE CHARACTERISTICS USING WIDER ANALYSED DATABASE

3.3.1. Source Levels

Broadside vessel source levels derived from all fully analysed vessel passages at each of the Summer 2013 AMAR stations are shown in Table 2.[8] "Fully analysed" vessel passages were those displaying interpretable interference fringes from which AMAR times of closest approach could be extracted independent of AIS-inferred passage times. In practice, this criterion limited fully analysed passages to those passing within about 7 km lateral range of the AMAR moorings. More distant passages could have been analysed using AIS passage times alone since any offsets between AIS and AMAR time bases become less critical at longer vessel ranges. However, it was considered prudent to maintain the above acceptance criteria since readily interpretable visible interference fringes signify both a strong vessel signal to ambient background noise ratio and a certain degree of simplicity in the propagation process. For vessel source level extraction, the standard frequency integration range of 20 – 1000 Hz encompassed the effective spectral range of most vessels studied. The frequency range also corresponded to that analysed by McKenna et al. (2012) for source levels from large vessels transiting the Santa Barbara Channel. For several vessels the frequency range was modified to incorporate

[8] Vessel identities were checked against vessel itineraries. In a couple cases where this was not possible there appeared no ambiguity associated with MMSI # so it is deemed quite probable that all listed vessels have been properly identified.

unusual spectral properties, namely: a) 50 – 1000 Hz for MidGul vessels *VESSEL "A"* and *VESSEL "C"* b) 20 – 2000 Hz for MidGul *VESSEL "F"*, and ShoHald vessels *VESSEL "O"*, *VESSEL "S"*, and *VESSEL "F"*. Source level alterations from use of the modified frequency ranges were small. Table 2 data were scaled visually from source level vs. range plots generated using ambient noise subtraction. The working plots (not shown) displayed separate curves for 10, 15.5, and 20 log R slant range TLs similar to those in Figs. 12 and 17.

3.3.2. SELs

In contrast to vessel source levels, which for the most part are inherent properties of the vessel alone[9], vessel SELs are also first order functions of the observation geometry, especially, the vessel range at closest passage and also vessel speed, slower vessels remaining within distance radii characterizing given minimum received noise levels for longer time intervals. The vessel SELs listed in Table 2 cover essentially complete vessel passages. The SELs were computed by numerical time and frequency integration of observed vessel spectral noise levels after background noise correction. The total analysed time window for vessel passage was usually 2.4 hours, approximately centered on the closest point of approach. The integration time window, which occasionally varied, was probably sufficient to ensure SELs within about 1 dB of the infinite time interval summation, although vessel noise signal fall-offs at longer ranges and the long term stability of the employed ambient background noise correction procedure are not well understood.

3.4. DISTINCTIVE VESSEL CHARACTERISTICS

The information provided in Table 2 was analyzed in several different ways:

1) Figure 20 shows vessel source level (dB re 1 μPa^2 @ 1 m) as a function of logarithmic vessel gross tonnage. Vessel type, simplified to "container", "dry cargo", "bulk carrier", "tankers" (oil and chemical tankers combined) or "other", has been colour-coded.

2) Figure 21 shows vessel source level vs. vessel speed (m/s), with vessel type colour-coded as above.

3) Figure 22 shows vessel source level vs. vessel speed (m/s), with the AMAR observing station colour-coded.

4) Figure 23 shows vessel source level vs. lateral range for all vessel types, with the AMAR observing station colour-coded.

[9] Vessel source levels likely vary with vessel speed but even if source levels are speed independent resultant SELs remain first order speed dependent.

Each of Figs. 20 – 23 consist of two plots: An upper plot shows vessel source levels computed using 15.5 log R slant range corrections while a lower plot shows the same quantities computed using 20 log R corrections.

From examination of the fully analysed vessel data (Table 2), the associated analytical plots listed above, and with additional reference to the wider list (not reproduced) of vessels detected within 20 km station radii, the following tentative conclusions are drawn:

1) Virtually all fully analysed vessels were large - only two vessels (both cargo) were < 10,000 GWT. No fishing vessels or small vessels of any type were detected within 20 km of any of the three mooring stations. Research vessel CCGS *HUDSON* appeared the smallest ship detected. Since *HUDSON* had just deployed the measurement AMARs on site or was otherwise involved in variable speed/course scientific survey activities, it did not qualify for detailed analysis. Any fishing vessels present within these radii either did not possess AIS beacons, their existing beacons were deactivated, or the beacons were undetected due to the sparse AIS reception coverage.

2) There appears little obvious correlation between vessel source level and vessel gross tonnage (Fig. 20). A suggestion of higher source levels associated with higher tonnage vessels on using the 15.5 log R corrections disappears when the 20 log R corrections are used. Any relationship between size and source level thus remains uncertain.

3) No overall relationship between source level and vessel speed in is clearly evident in Fig. 21 although a suggestive linear relationship between vessel speed and decibel source level appears when data is restricted to container ships alone. Our data would indicate that container ships and bulk carriers are, on average, noisier than tankers and cargo ships. Comparing Fig. 21 to the similar plot (Fig. 5) in the McKenna et al. (2012) Santa Barbara Channel study is instructive. A similar clustering in characteristic speeds between container ships (about 11 m/s in the Santa Barbara study) and bulk carriers, cargo, and various tanker types, all combined (6 – 8 m/s in the Santa Barbara study) was observed. The source levels for container ships in the Santa Barbara study (average = 185.5 dB) were also comparable to the source level estimates in our study (184.3 and 186.1 dB on using 15.5 and 20 log R corrections respectively). However, in the Santa Barbara study, tankers displayed source levels several dB lower (average = 181.3 dB over all tanker types) than in our study (average =183.1 and 184.6 dB for 15.5 and 20 log R corrections respectively). Bulk carrier source levels in the Santa Barbara study were also slightly lower (average = 185.7 dB) than for similar vessel types in our current study (average = 186.0 and 187.0 dB for 15.5 and 20 log R corrections respectively). The correlations of source levels with ship type appeared clearer (i.e. characterized by less scatter) in the Santa Barbara study than in our results.

It is evident in Fig. 21 that 20 log R TL corrections resulted in less source level scatter for all major vessel classes than use of 15.5 log R corrections (though still more scatter than observed by McKenna et al. 2012). However, on considering decibel-averaged vessel source levels, our 15.5 log R corrected source levels (average = 184.1 dB) appeared to better agree with the average levels observed by McKenna et al. (182.8 dB over all vessel types or 183.2 dB on eliminating vehicle carriers - a vessel class not encountered in our fully analysed data). Our 20 log R corrected source levels averaged 1.5 dB higher (185.6 dB) than those corrected using 15.5 log R slant range dependencies.

4) Some systematic correlation of vessel source levels with the specific AMAR location is evident in Fig. 22. GulSho station detected no fully analysed high speed vessels, all but one of the analysed vessels consisting of relatively low speed tankers.

5) A fall-off in computed vessel source levels with increasing lateral observation range (data lumped for all stations) is apparent on using15.5 log R slant range corrections (Fig. 23), but a similar fall-off is less evident or absent on using 20 log R corrections (same figure). This may indicate a superior reality for the 20 log R corrections, it being remembered that the source level scatter in Fig. 22 was also reduced on using the 20 log R corrections. Corrections based upon a 20 log R dependence were employed in the studies of McKenna et al. (2012) and Bassett (2010), as well as suggested much earlier by Urick (1975). It might also be questioned whether a broad dip at about 3 – 4 km range may be present. It will be remembered that our empirical TL relationships are only frequency independent approximations to the P.E. modelling. Note the detailed P.E. results in Figs. 7 and 8 do suggest sharp increases in TL at depth within this distance range especially at the low frequency end of the ship noise spectrum. This might well arise from interference between the direct and first bottom bounce signal paths at depth, a feature perhaps excessively obscured in our empirical TL fits and revealing the fundamental limitations of the simplistic approach.

Some general observations can also be made about vessel source levels vs. observation aspect. Decibel-averaged **broadside** vessel RMS source levels over all stations were 182.1, 184.1, and 185.6 dB re 1 uPa^2 @ 1m on assuming 10, 15.5, and 20 log R slant range corrections respectively, with limited indirect evidence that the 20 log R derived corrections might be the more accurate. The attempt was made to compare vessel acoustic source levels derived in vessel approach, broadside, and in departure aspects. As with the two examples already considered, a marked tendency was observed in the wider database for source levels to be lower-than-broadside in approach and higher-than-broadside in departure. This was concluded from visual inspection of source level vs. time plots, with particular attention to extended time periods during which SLs were relatively stable. Using 20 log R corrections, source levels in approach, broadside, and in departure averaged 183.5, 185.6, and 187.0 dB re 1 μPa^2 @ 1 m respectively. The quoted lumped approach and departure source levels are probably not overly meaningful because of the absence of stringent controls on vessel aspect associated with differing passage

distances and vessel speeds. If we restrict analysis to the five cases where the vessel passed within 1 km lateral range of the mooring, where the transition from near-bow to near-stern aspect occurred relatively quickly, the corresponding SLs are 183.6, 184.6, and 185.8 dB respectively (i.e. near-stern aspect SLs exceed near-bow SLs by about 2.2 dB). This difference is smaller than the 3.5 dB difference for the entire fully analysed dataset without regard to the minimum range at passage. McKenna et al. (2012) reported considerably larger approach vs. departure SL differences of 5 to 10 dB. Possibly the deep receiver depth of the AMAR instruments minimized bow vs. stern aspect SL differences especially for very close passages by minimizing propeller sound shadowing by the hull on approach.

3.5. SOURCES OF UNCERTAINTY

Many sources of uncertainty in this study have already been discussed. For example, propagation path bathymetries were not well constrained especially for vessels quite distant to the acoustic mooring sites. Analysed vessels travelled at highly variant headings and passed at a variety of ranges to the three different moorings. While mooring depths were roughly consistent, the surrounding bathymetries were far from flat and featureless resulting in different ocean-bottom boundary conditions affecting propagation on different ship passages and even for differing portions of the same passage. Range dependent bathymetries were not accounted for in our propagation model. While bathymetries in the comparative Santa Barbara Channel study (McKenna et al. 2012) did vary, individual vessel passage geometries were quite reproducible, ships moving in a more-or-less fixed lane, 3 km (slant range) at closest passage, with water depth about 580 m.

Another possible source of uncertainty, also related to the spatially variant bathymetry, is the dependence on observed multi-path acoustic interference phenomena (i.e. sonogram fringes) to define the precise times of closest vessel passage. While this methodology should work reasonably well for flat bottoms, biases are undoubtedly introduced by the spatially variant bathymetries. Observed asymmetries in ship passage sonograms also hint this could be the case. Inferred deviations between AIS and acoustic-derived passage times at the various stations did not vary in totally systematic manners over the study period. Therefore, it remains unclear whether true AMAR clock drift was consistently resolved, our working assumption, or, to the contrary, timing limitations innate to the interference fringe technique itself were being observed. Unfortunately, no attempts were made on AMAR recovery to measure total accumulated clock drift. More stable AMAR clocks are possible but at the expense of significantly shorter battery life.

Acoustic propagation, especially at multi-kilometer lateral ranges, is strongly governed by the prevailing sound speed structure. Earlier studies associated with the eastern Scotian Shelf/Slope 2003 Marathon Seismic survey had shown that sound speeds in the upper 200 m of water column change systematically and rapidly in the May – June period. This was mainly a consequence of the growth of the shallow seasonal thermocline, but moving ocean frontal boundaries between contrasting Scotian Shelf and Scotian Slope waters also occasionally induced rapid fluctuations in water column

temperature structure. Such changes are not accounted for in our P.E. based propagation model where only a single composite sound speed profile was used to derive TL range dependencies.

More fundamentally, we have assumed TLs to be frequency independent over the frequency range of spectrally significant ship noise and to be simple logarithmic functions of range. While these assumptions are a major convenience in enabling very simple frequency independent TL corrections to be applied to spectrally lumped broadband vessel sound pressure levels, the P.E. modelling results show these are only fair approximations at the longer vessel ranges and lowest acoustic frequencies considered. There is little reason to believe the real-world situation is better than that modelled. An improved sound source representation for inclusion in the P.E. model would also be beneficial. Clearly, real vessels are not acoustic point sources at a single fixed 10 m depth.

4. ACKNOWLEDGEMENTS

Many who have contributed to this work have been acknowledged in the parent document. They include Jay Barthelotte and Adam Hartling of BIO's Ocean Physics Section and Pierre Clement, of BIO's Coastal Ecosystem Science Division. Pierre directly furnished exactEarth AIS data to us along with invaluable advice regarding its characteristics. The officers and crew of our research vessel, CSS HUDSON, performed proficiently and the Senior Scientists generously and effectively accommodated our specific needs. Bruce Martin, Applied Science Manager, JASCO Applied Sciences Ltd. is again acknowledged as our manufacturer liaison.

Sincerely appreciated and of great value were the critiques of advanced drafts of this manuscript by David Barclay, Department of Oceanography, Dalhousie University and Pamela Emery, Ocean and Ecosystem Sciences Division, BIO. However, the authors should make clear that the reviewers served in an advisory capacity only and that the report's contents should neither be considered as necessarily reflecting their views nor as necessarily carrying their full endorsement.

Archived Environment Canada meteorological historical from Sable Island was accessed through the Govt. of Canada online data portal at: http://climate.weather.gc.ca/historical_data/search_historic_data_e.html - link last verified 15 June 2016. Principal computations were performed using Lahey-Fujitsu Fortran 95 v 5.6 with integrated Winteracter v 8.0. Graphics were provided by Matlab v 5.1.0.421.

This work was supported by DFO SPERA (**S**trategic **P**rogram for **E**cosystem-Based **R**esearch and **A**dvice) funding.

5. REFERENCES

Arveson, P.T. and Vendittis, D.J. 2000. Radiated noise characteristics of a modern cargo ship. J. Acoust. Soc. Am. 107(1): 118 – 129.

Bassett, C. 2010. Underwater ambient noise at a proposed tidal energy site in Puget Sound. Thesis (M.Sc. in Mechanical Engineering) University of Washington, Seattle, Wash. vii + 58 p. Available online: http://depts.washington.edu/nnmrec/docs/20100528_BassettC_thesis_UnderwaterNoise.pdf (accessed 17 June, 2015).

Clay, C.S., and Medwin, H. 1977. Acoustical oceanography principles and applications. John Wiley & Sons, New York. 544 p.

Cochrane, N.A. 2007. Ocean bottom acoustic observations in the Scotian Shelf Gully during an exploration seismic survey – a detailed study. Can. Tech. Rep. Fish. Aquat. Sci. 2747: viii + 73 p.

Cochrane, N.A., and Moors-Murphy. H. 2017. Passive acoustic monitoring on the eastern Nova Scotian Shelf Slope and in the Gully Marine Protected Area. Can. Tech. Rep. Fish. Aquat. Sci. 3236. In press.

Collins, M.D. 1992. A self starter for the parabolic equation method. J. Acoust. Soc. Am. 92(4): 2069 – 2074.

Collins, M.D. 1993. A split-step Padé solution for the parabolic equation method. J. Acoust. Soc. Am. 93(4): 1736 - 1742.

Jensen, F.B., Kuperman, W.A., Porter, M.B., and Schmidt, H. 2000. Computational ocean acoustics. AIP Series in Modern Acoustics and Signal Processing. Springer-Verlag, New York. 578 p.

Mackenzie, K.V. 1981. Nine-term equation for sound speed in the oceans. J. Acoust. Soc. Am. 70: 807-812.

McKenna, M.F., Ross, D., Wiggins, S.M., and Hildebrand, J.A. 2012. Underwater radiated noise from modern commercial ships. J. Acoust. Soc. Am. 131(1): 92 – 103.

Raymond, E.S. 2014. AIVDM/AIVDO protocol decoding. Version 1.46, Aug. 2014. Latest version on-line: http://catb.org/gpsd/AIVDM.html (accessed 09 March, 2016).

Simard, Y., Roy, N., Giard, S., and Yayla, M. 2014. Canadian year-round shipping traffic atlas for 2013: Volume 1, East coast marine waters. Can. Tech. Rep. Fish. Aquat. Sci. 3091(Vol. 1) E: xviii + 327 p.

Urick, R.J. 1975. Principles of underwater sound. McGraw-Hill Book Company, New York. 384 p.

Table 1. Summer 2013 AMAR mooring deployment details.

Mooring	Lat N	Long E	Bottom Depth m	Deploy DOY
MidGul:	43.86225	-58.90997	1580	126.98958
GulSho:	43.86376	-58.58818	1583	127.07708
ShoHald:	44.09772	-58.05636	1545	127.19097

Table 2. Vessels passing sufficiently proximate to the three Summer 2013 AMAR stations to permit confident estimates of vessel acoustic source level.

MMSI #	Vessel	Date	Type	GWT	Speed	Course	Nearest	10 logR	15.5 logR	20 logR	SEL
MidGul		**2013**			**kts**	**E of N**	**km**	**SL dB**	**SL dB**	**SL dB**	**dB**
xxxxxxxxx	*VESSEL "A"*	06/22	Container	25672	13.33	243.2	3.925	173	176	179	144
xxxxxxxxx	*VESSEL "B"*	05/24	Dry Cargo	4200	12.12	57.2	0.023	180	180	180	148
xxxxxxxxx	*VESSEL "C"*	06/12	Container	53822	17.45	62.8	2.381	182	185	187	151
xxxxxxxxx	*VESSEL "D"*	06/18	Bulk Carrier	16807	11.31	187.2	6.382	183	188	190	150
xxxxxxxxx	*VESSEL "E"*	06/08	Bulk Carrier	44146	15.20	240.6	1.881	188	190	190	158
xxxxxxxxx	*VESSEL "E"*	06/15	Bulk Carrier	44146	10.28	58.7	0.274	180	180	180	150
xxxxxxxxx	*VESSEL "F"*	05/23	Container	54415	21.33	249.1	1.131	190	190	190	158
GulSho		**2013**									
xxxxxxxxx	*VESSEL "G"*	06/12	Tanker	30638	13.60	222.5	2.483	182	184	186	153
xxxxxxxxx	*VESSEL "H"*	06/25	Oil Tanker	58418	11.04	43	1.72	186	187	187	153
xxxxxxxxx	*VESSEL "I"*	05/21	Gen. Cargo	5629	10.9	352.5	5.052	180	183	187	151
xxxxxxxxx	*VESSEL "J"*	06/06	Oil Tanker	13239	13.4	176.2	2.439	180	182	183	150
xxxxxxxxx	*VESSEL "K"*	05/26	Oil Tanker	35711	12.8	2	6.645	175	179	181	146
xxxxxxxxx	*VESSEL "L"*	06/13	Tanker	26459	13.3	1.7	0.377	186	186	186	155
xxxxxxxxx	*VESSEL "L"*	06/18	Tanker	26459	14.15	181.6	0.421	187	187	187	155
xxxxxxxxx	*VESSEL "M"*	06/23	Oil Tanker	157098	11.91	314.0	2.713	180	182	184	150
xxxxxxxxx	*VESSEL "N"*	05/19	Chem. Tank.	12358	11.20	0.0	5.664	180	183	187	150
ShoHald		**2013**									
xxxxxxxxx	*VESSEL "O"*	06/21	Bulk Carrier	15899	13.02	152.0	0.763	190	190	190	160
xxxxxxxxx	*VESSEL "C"*	06/12	Container	53822	17.13	63.5	4.427	180	182	185	149
xxxxxxxxx	*VESSEL "P"*	06/12	Container	66462	19.77	289.0	2.368	184	186	187	152
xxxxxxxxx	*VESSEL "Q"*	06/16	Bulk Carrier	16833	11.37	162.7	5.361	179	182	185	150
xxxxxxxxx	*VESSEL "R"*	05/10	Container	40542	17.60	285.6	6.532	180	185	188	148
xxxxxxxxx	*VESSEL "S"*	06/04	Cable	12184	12.30	59.1	1.853	186	187	188	151
xxxxxxxxx	*VESSEL "F"*	05/23	Container	54415	19.88	248.9	1.504	185	186	187	151
xxxxxxxxx	*VESSEL "N"*	05/12	Chem. Tank.	12358	12.46	178.1	4.812	174	178	180	146

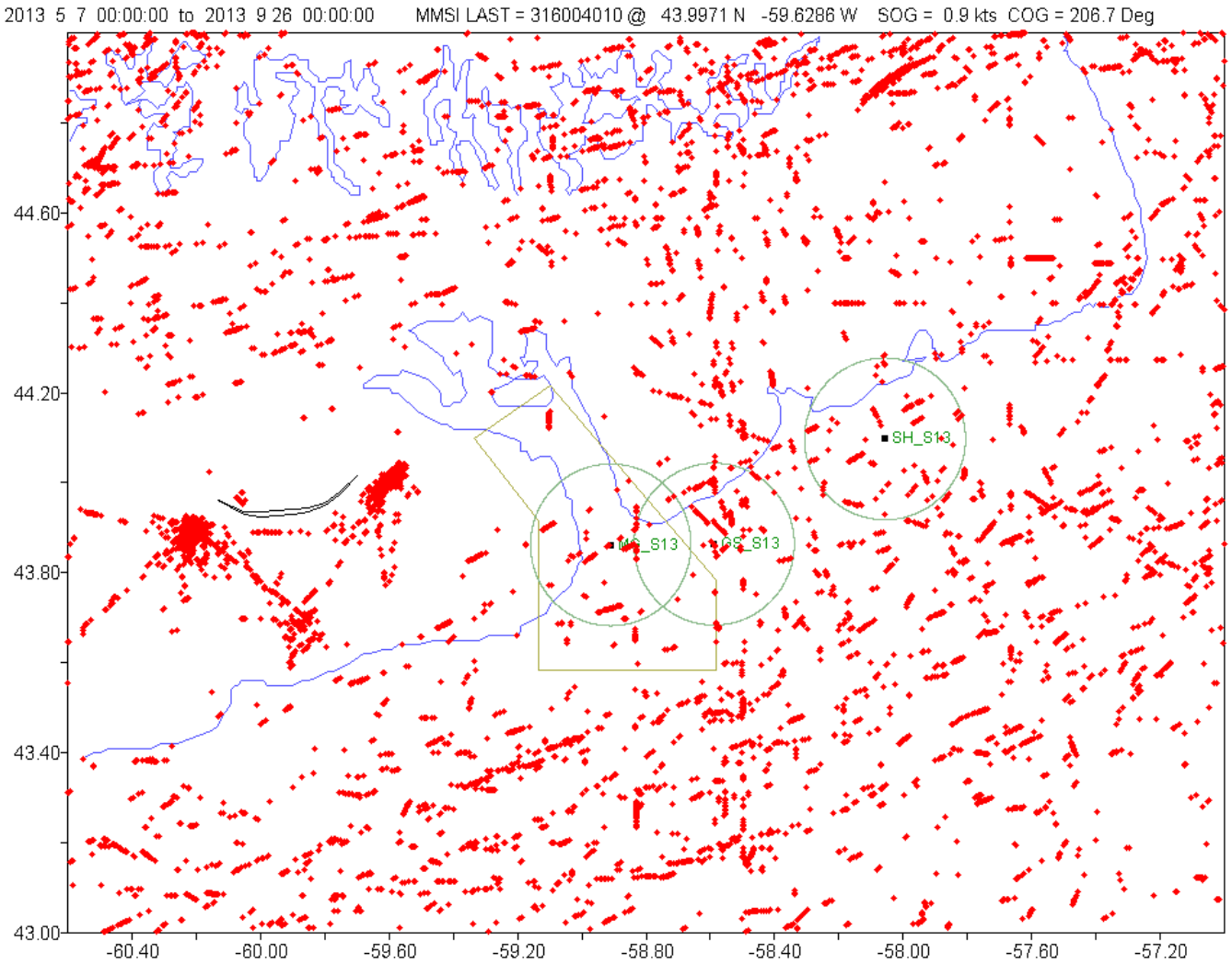

Figure 1. AIS ship positions (Channel A): Summer 2013 deployment 07 May – 30 June 2013.

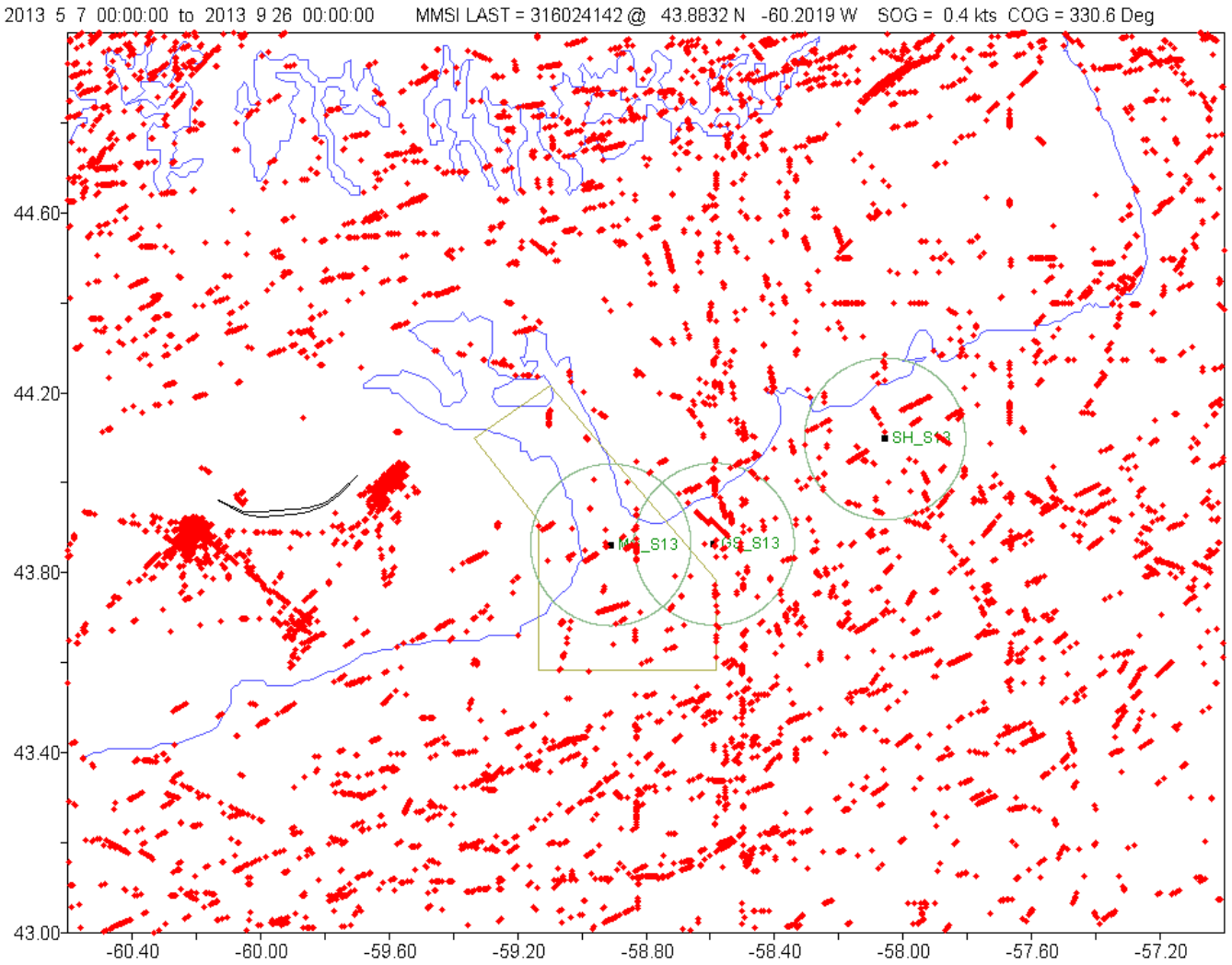

Figure 2. AIS ship positions (Channel B): Summer 2013 deployment 07 May – 30 June 2013.

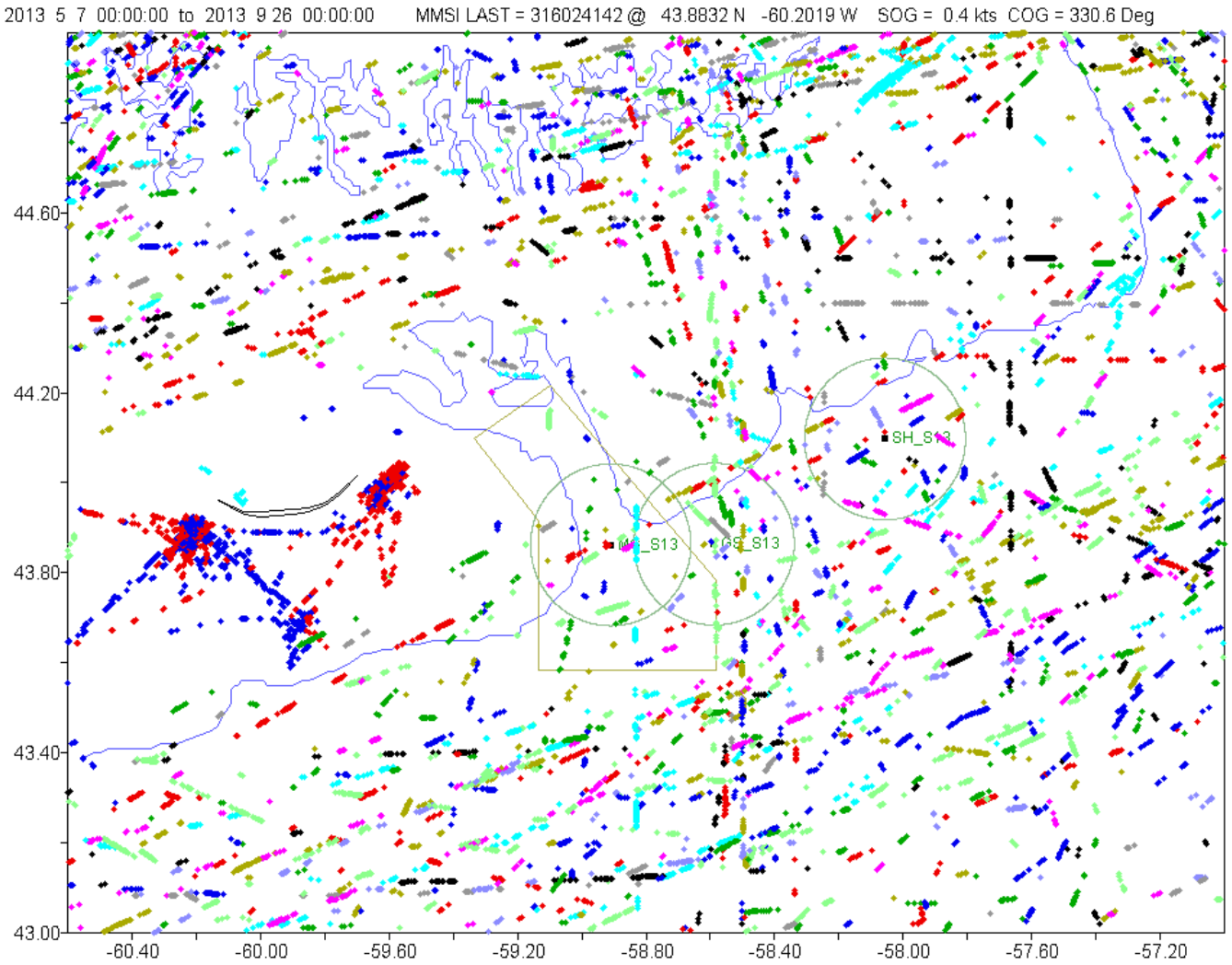

Figure 3. AIS ship positions (Channels A and B combined). Summer 2013 deployment 07 May 2013 – 30 June 2013. Ship positions have been colour-coded in accordance with the 6th digit of the vessel MMSI #.

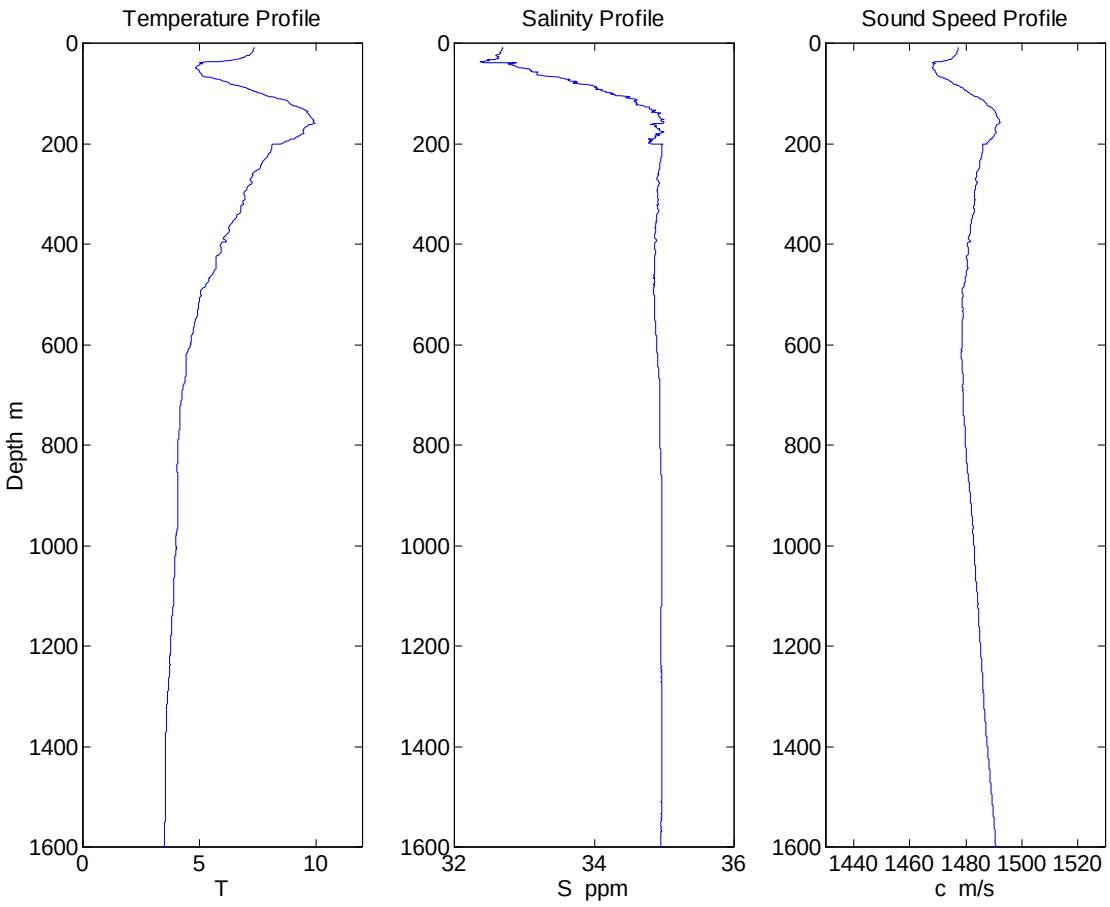

Figure 4. Combined 23 May 2013 (top 200 m) and 25 May 2003 (deeper) Scotian Slope temperature and salinity profiles and the resultant computed sound speed profile.

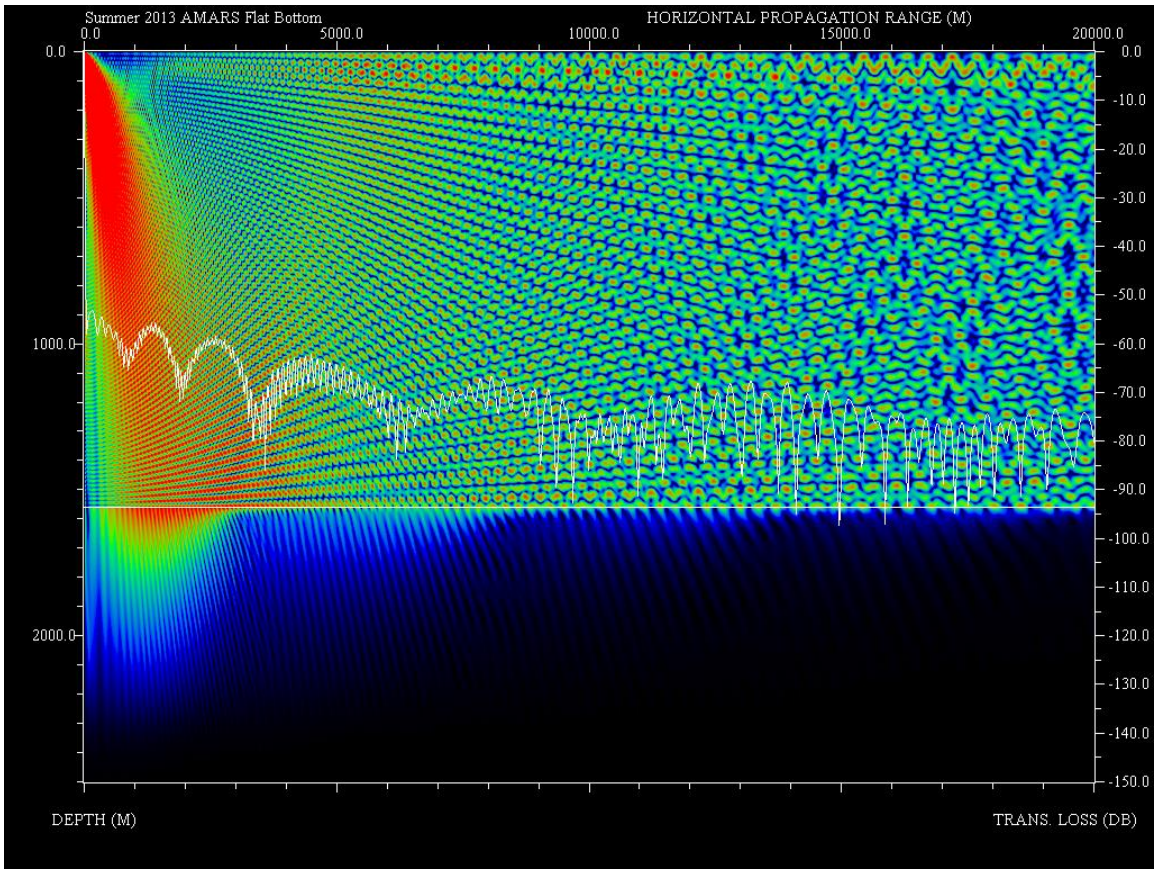

Figure 5. P.E. modeled transmission loss at 50 Hz in dB (white curve, RH scale) from a wide-angle acoustic source placed at 10 m depth (LH scale) to a receiver at 1500 m depth positioned at variable lateral ranges (horizontal scale) from the source. Plotted background colour corresponds to the P.E. computed sound pressure level with a cylindrical spreading component removed (increasing black to red).

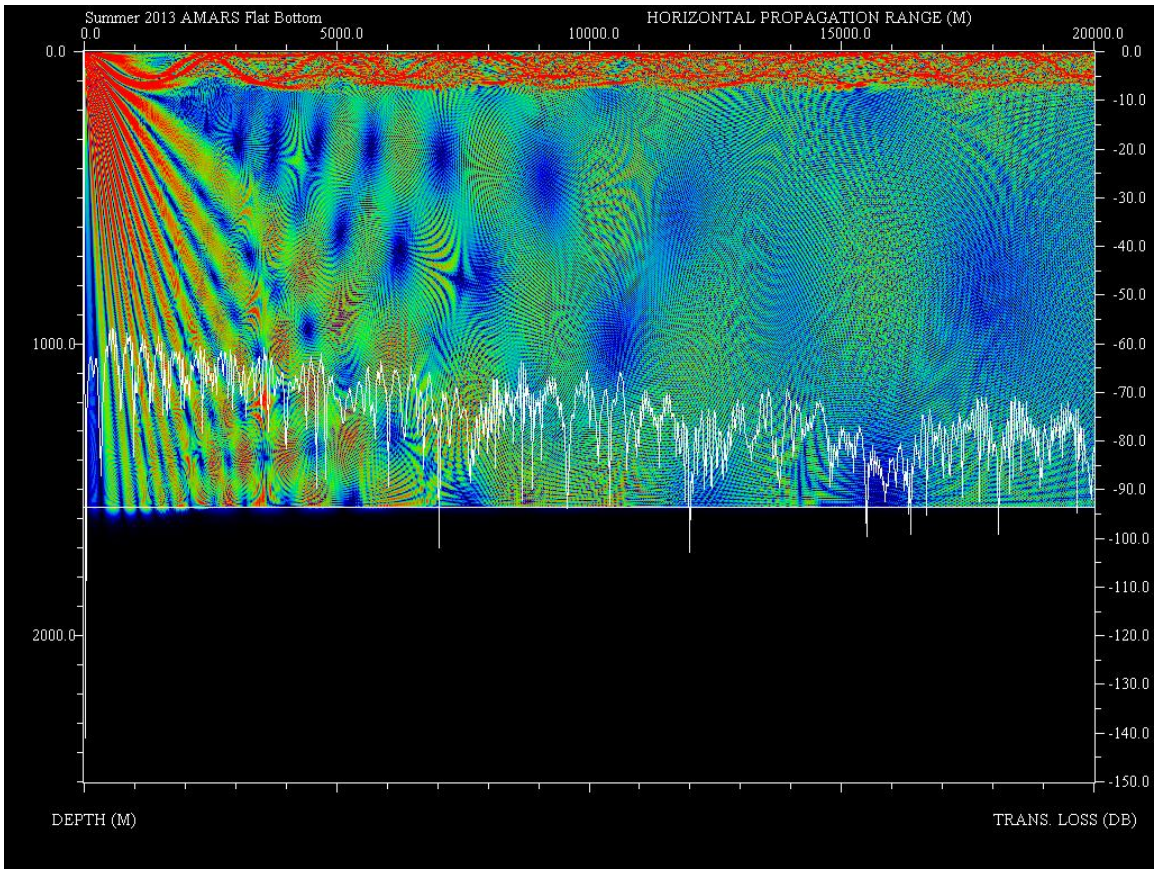

Figure 6. P.E. modeled transmission loss at 1000 Hz in dB (white curve, RH scale) from a wide-angle acoustic source placed at 10 m depth (LH scale) to a receiver at 1500 m depth positioned at variable lateral ranges (horizontal scale) from the source. Plotted background colour corresponds to the P.E. computed sound pressure level with a cylindrical spreading component removed (increasing black to red).

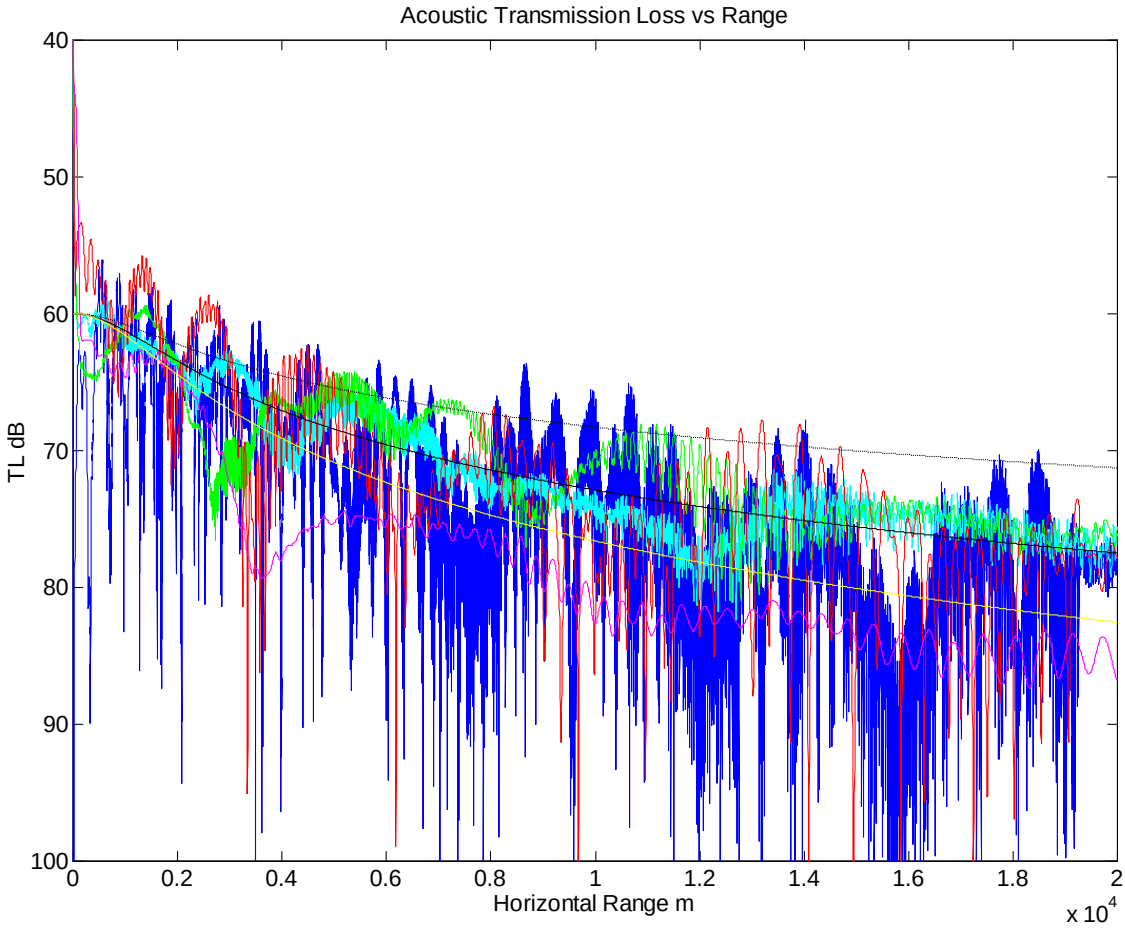

Figure 7. Decibel TL from an acoustic source at 10 m depth to a receiver at 1500 m depth plotted as a function of linear horizontal (lateral) source-to-receiver range. TL has been computed for 5 differing 1/3 octave width frequency bands centered at 20 (magenta), 50 (dark blue), 150 (cyan), 400 (green), and 1000 Hz (red). Proposed overall fitting curves for the following **slant range** dependencies (see Fig. 8) are superimposed: 10.0 log (slant range) – black dashed line; 15.5 log (slant range) – black solid line; and 20.0 log (slant range) – yellow line.

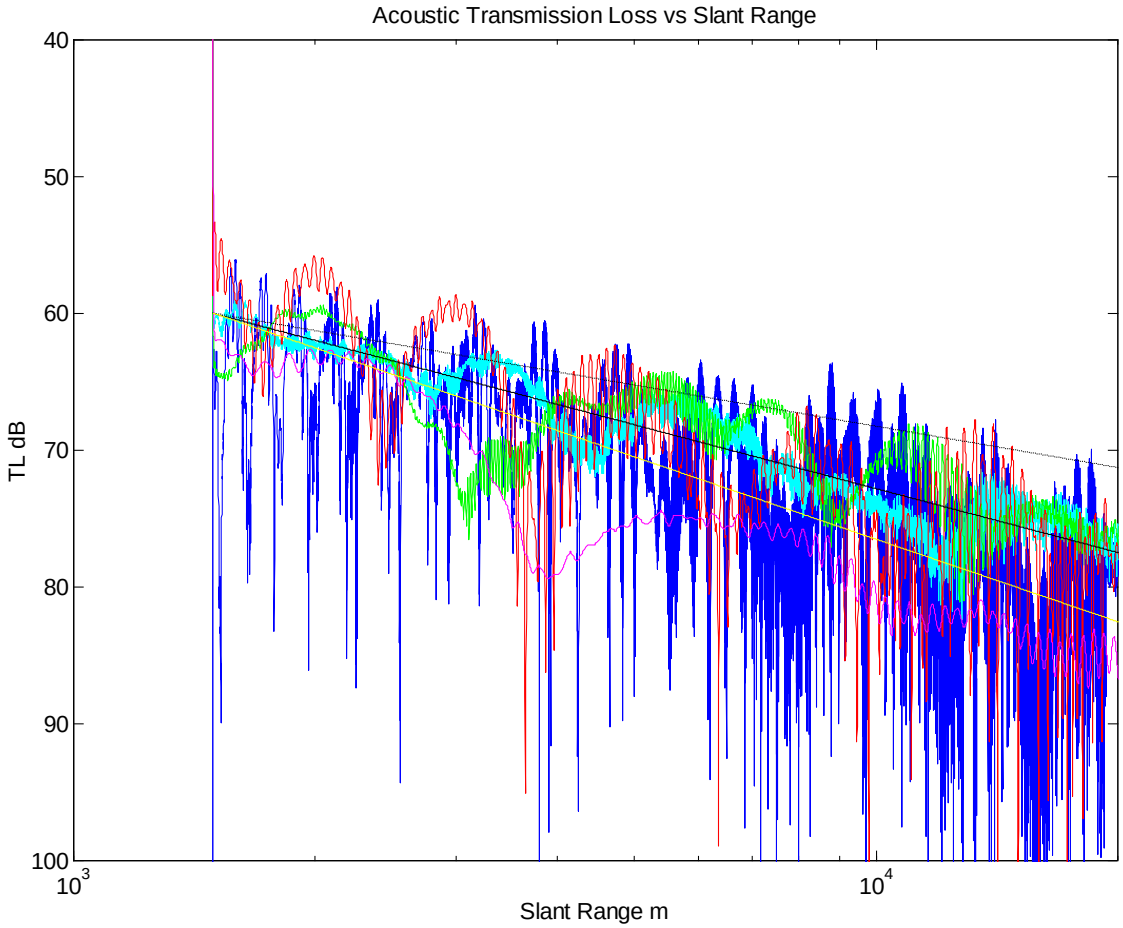

Figure 8. Decibel TL vs. logarithmic scale slant range for the 5, 1/3 octave bands as plotted in Fig. 7 with proposed overall fitting lines. Superimposed fitting lines assume a 60.0 dB TL when the receiver is placed directly below the source (i.e. at 0 m lateral range) and the following slant range dependencies: 10.0 log (slant range) – black dashed line; 15.5 log (slant range) – black solid line; and ≈20.0 log (slant range) – yellow line

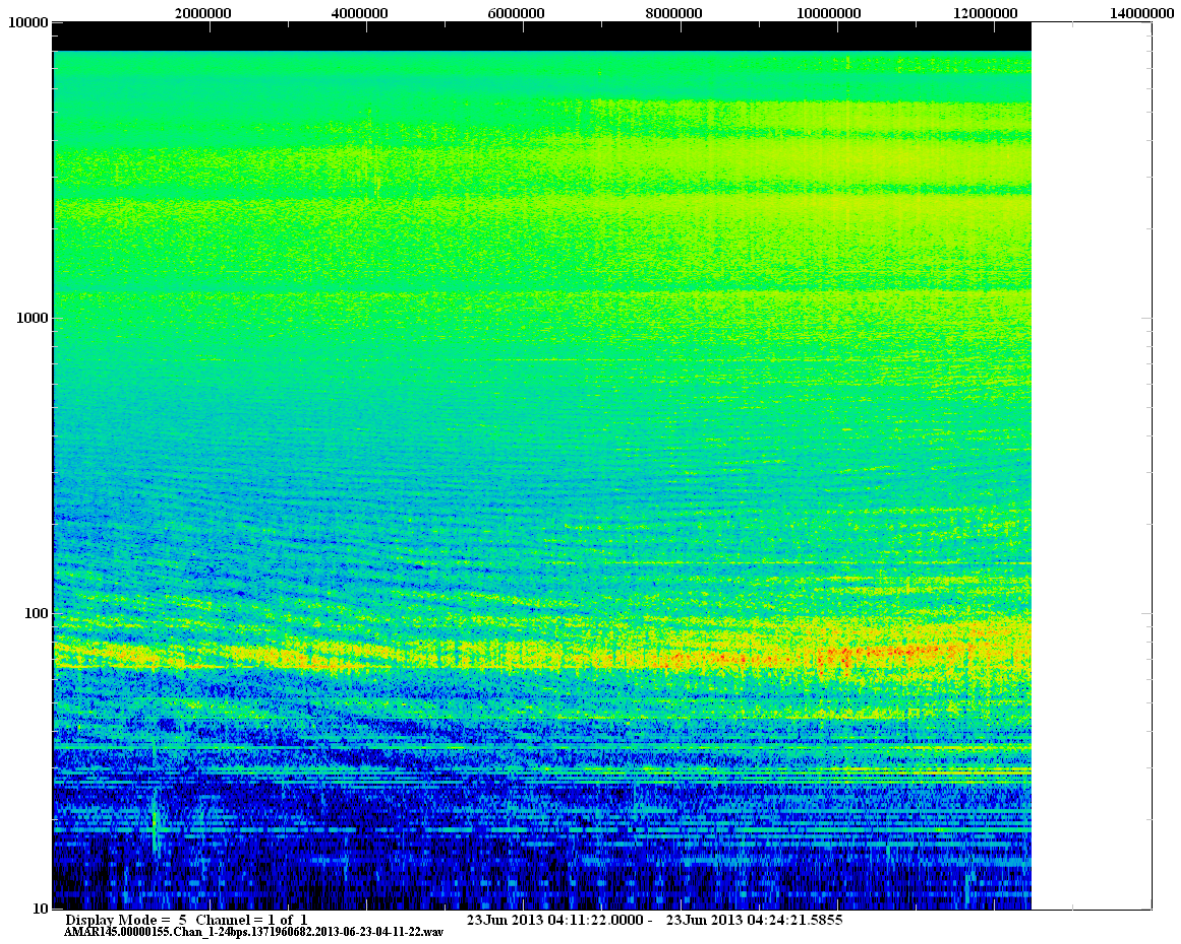

Figure 9. High resolution sonogram of central portion of *VESSEL "M"* passage showing appearance of multipath interference fringes (concave downwards). Vessel noise has both continuous and line components. Total (sonogram) time duration = 780s (0.00903 days), time resolution ≈ 2 s, frequency resolution = 0.49 Hz (for higher frequencies limited by pixel resolution). Data pre-whitened by application of digital 1st derivative to boost higher frequency intensities. Complex photographic intensity mappings have been employed to maximize fringe visibilities. Data not corrected for AMAR frequency response.

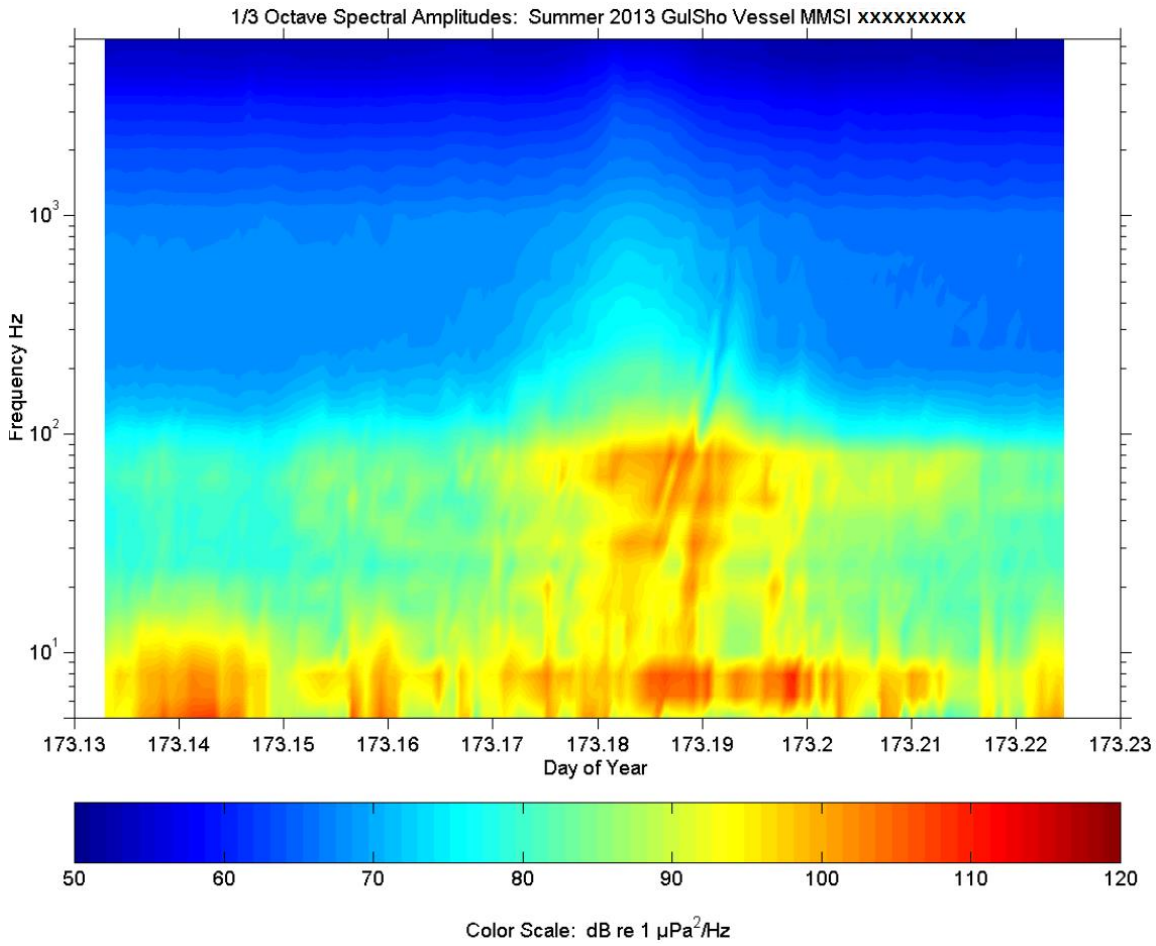

Figure 10. 1/3 Octave power spectrum of *VESSEL "M"* during close passage to GulSho mooring on 23 June 2013 (2.713 km minimum lateral range at DOY 173.18194 AMAR time).

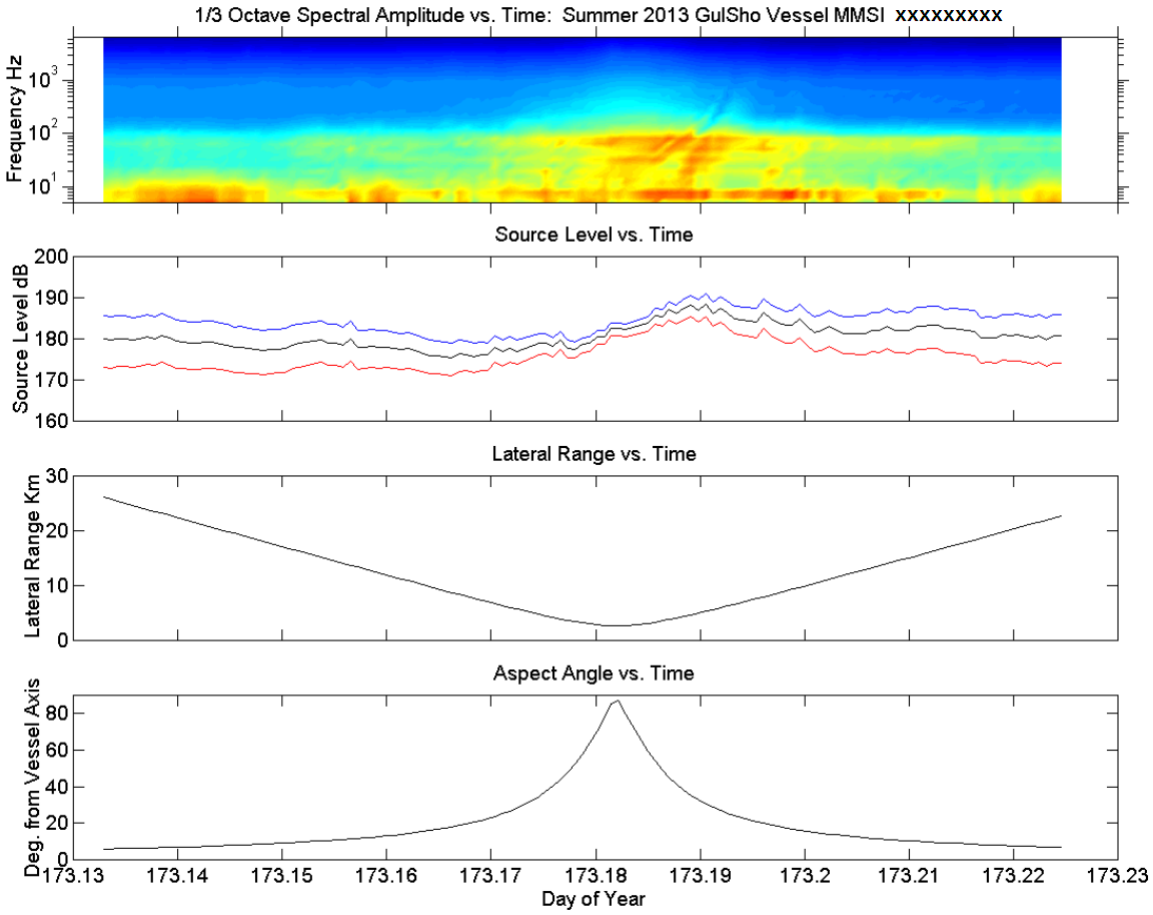

Figure 11. Vessel 1/3 octave acoustic spectral levels observed at GulSho mooring as a function of AMAR time as detailed in Fig. 10 (1st plot). Derived vessel acoustic source levels in dB re 1 μPa^2 @ 1 m using TL dependencies of 10.0 log (slant range) in red, 15.5 log (slant range) in black, and 20 log (slant range) in blue vs. time (2nd plot). Vessel lateral range (3rd plot) and observation angular aspect relative to the surface projection of the mooring (4th plot) vs. AMAR time. Vessel was *VESSEL "M"* (MMSI # xxxxxxxxx), average speed 11.91 knots, with closest approach 2.713 km lateral range at DOY 173.18194.

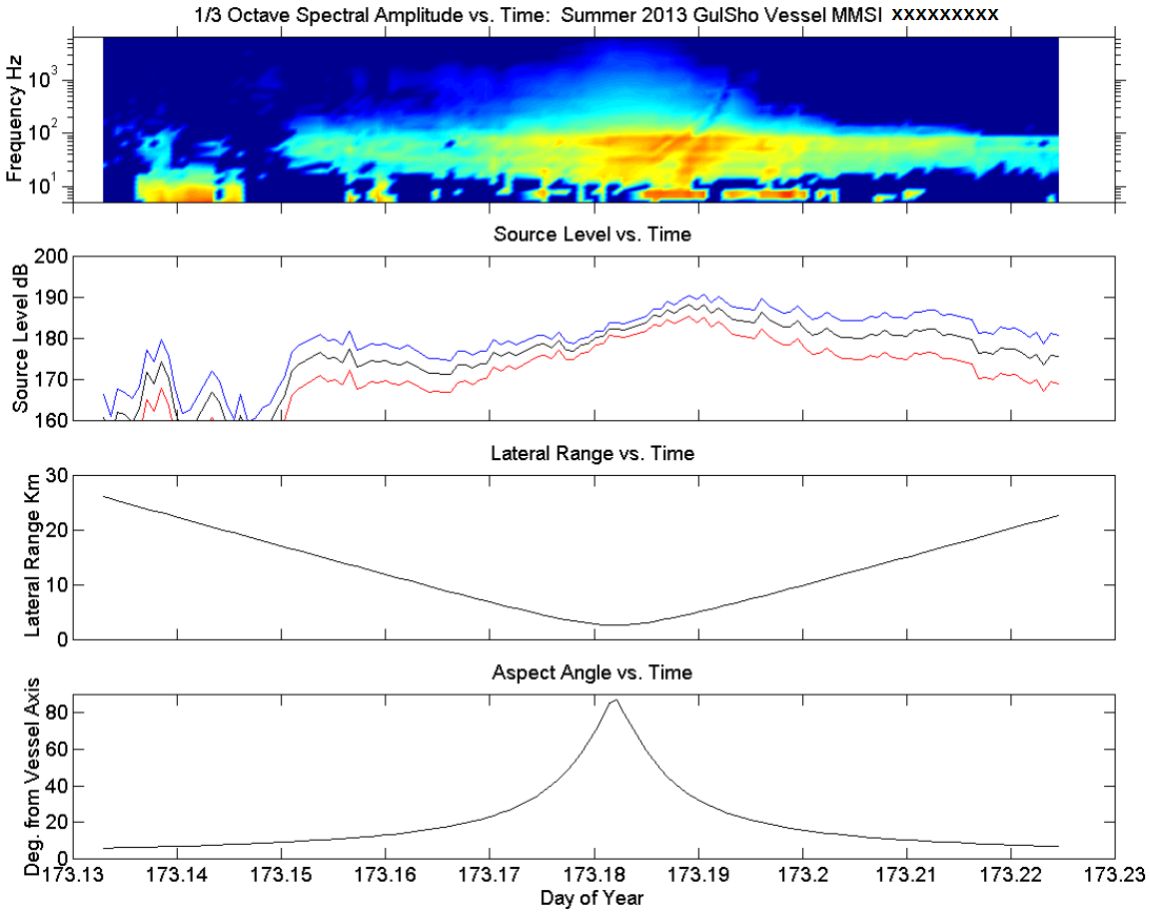

Figure 12. The same plots as in Fig. 11 except that the estimated ambient noise background obtained by averaging over the first 10 spectral estimates has been initially subtracted.

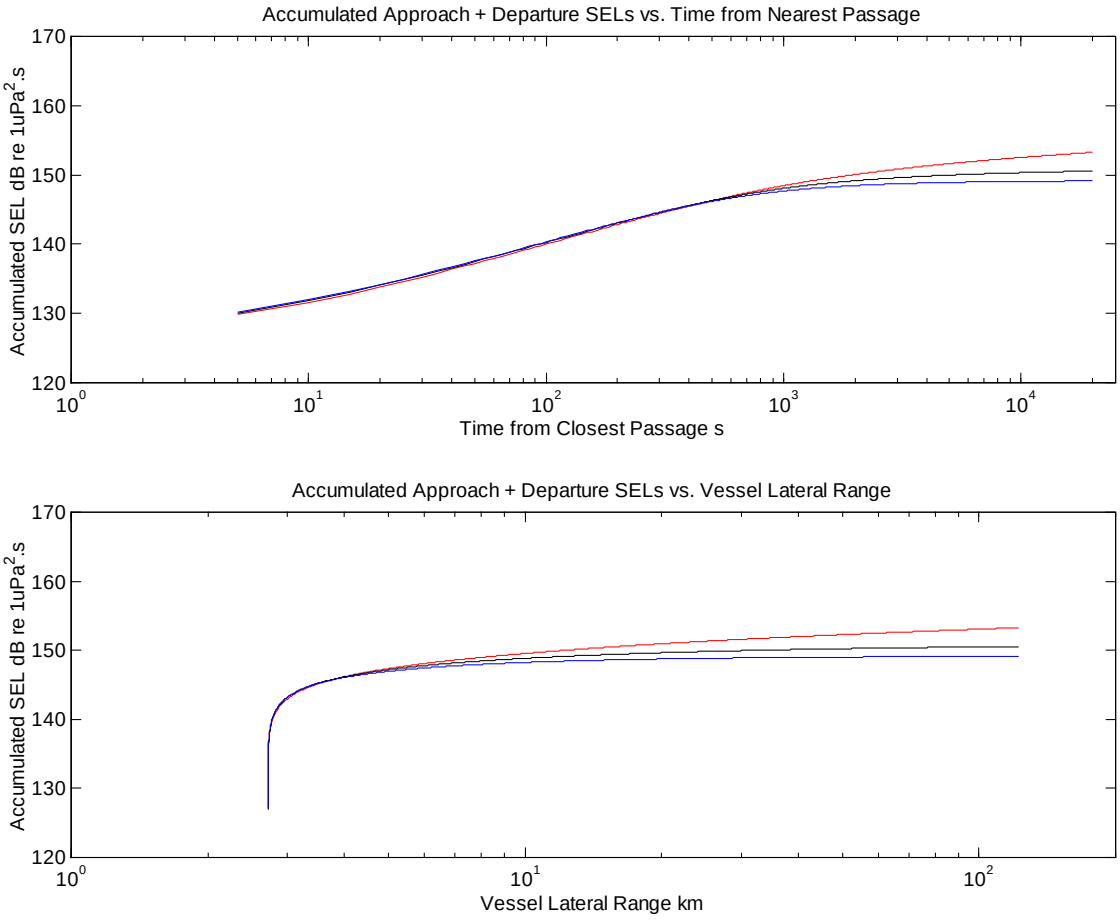

Figure 13. Mooring receiver theoretical cumulative SEL vs. time from closest passage (top) and theoretical cumulative SEL vs. vessel maximum lateral range (bottom) computed for *VESSEL "M"* (MMSI # xxxxxxxxx), transect passing near GulSho on 23 June 2013. Separate curves are computed assuming 10 log R (red), 15.5 log R (black) and 20 log R (blue) slant range dependencies.

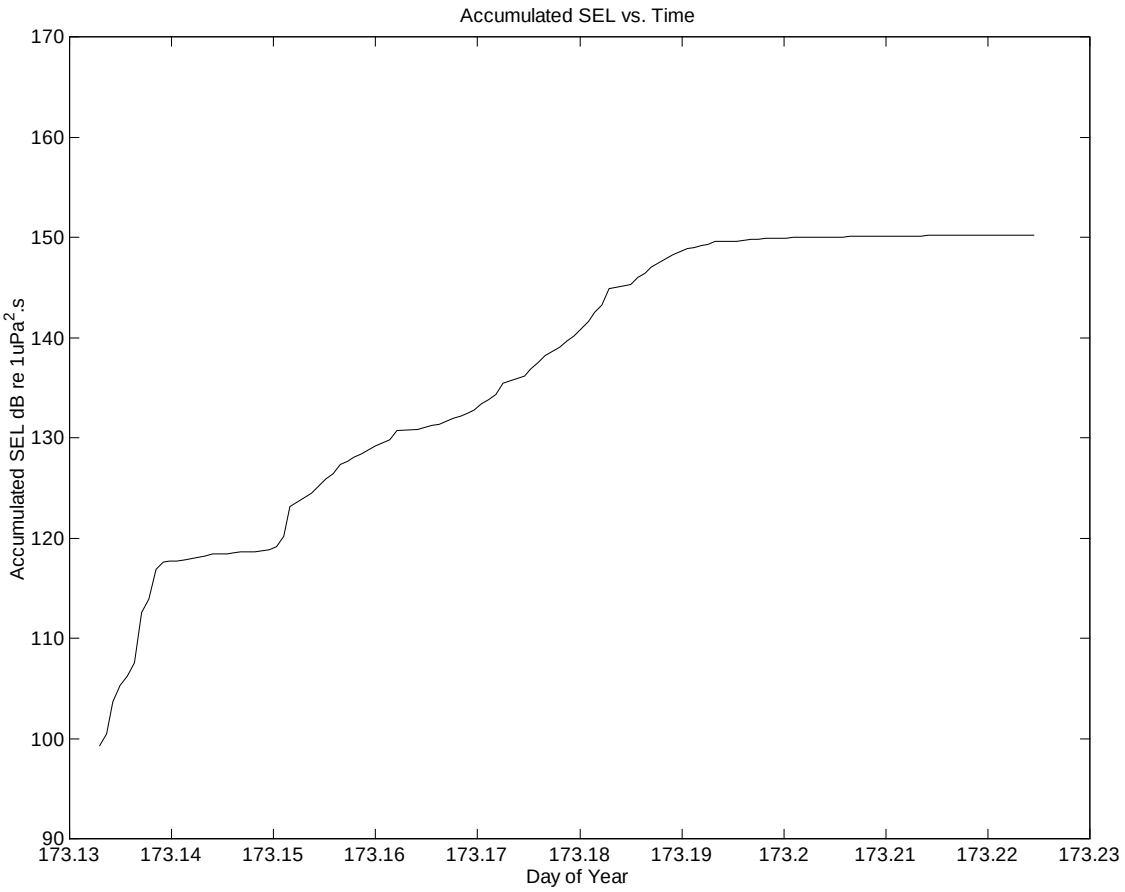

Figure 14. Experimentally computed SEL for *VESSEL "M"* (MMSI # xxxxxxxxx) passage of GulSho on 23 June 2013, utilizing successive 1/3 octave spectral estimates and the identical noise subtraction procedure and the identical considered spectral sub-range as used in the estimation of source levels. Vessel passage closest approach occurred at DOY 173.1819. SEL integration time extends from DOY 173.1329 to DOY 173.2246 corresponding to 4237 s prior to closest passage to 3683 s post closest passage.

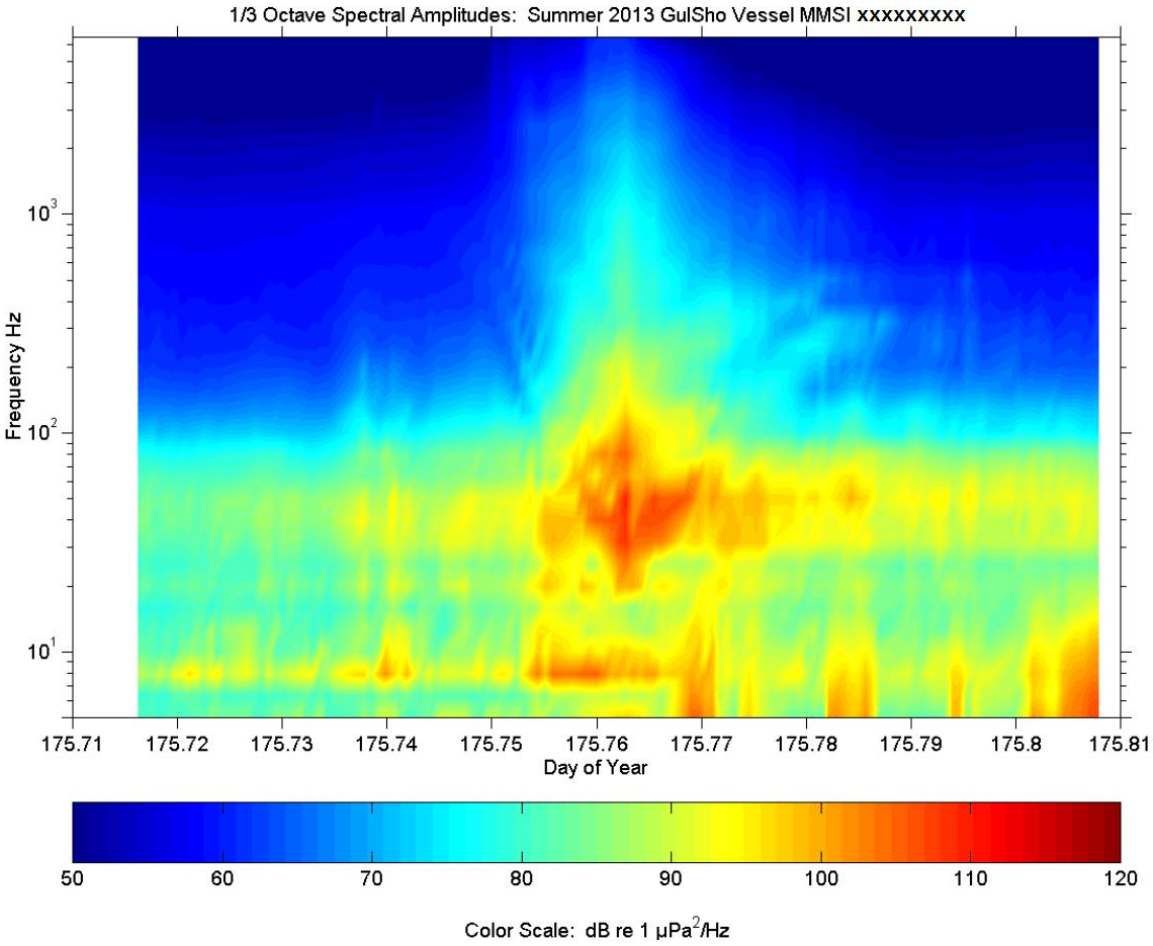

Figure 15. 1/3 Octave power spectrum of vessel *VESSEL "H"* during close passage to GulSho mooring on 25 June 2013 (1.720 km minimum lateral range at DOY 175.76198 AMAR time).

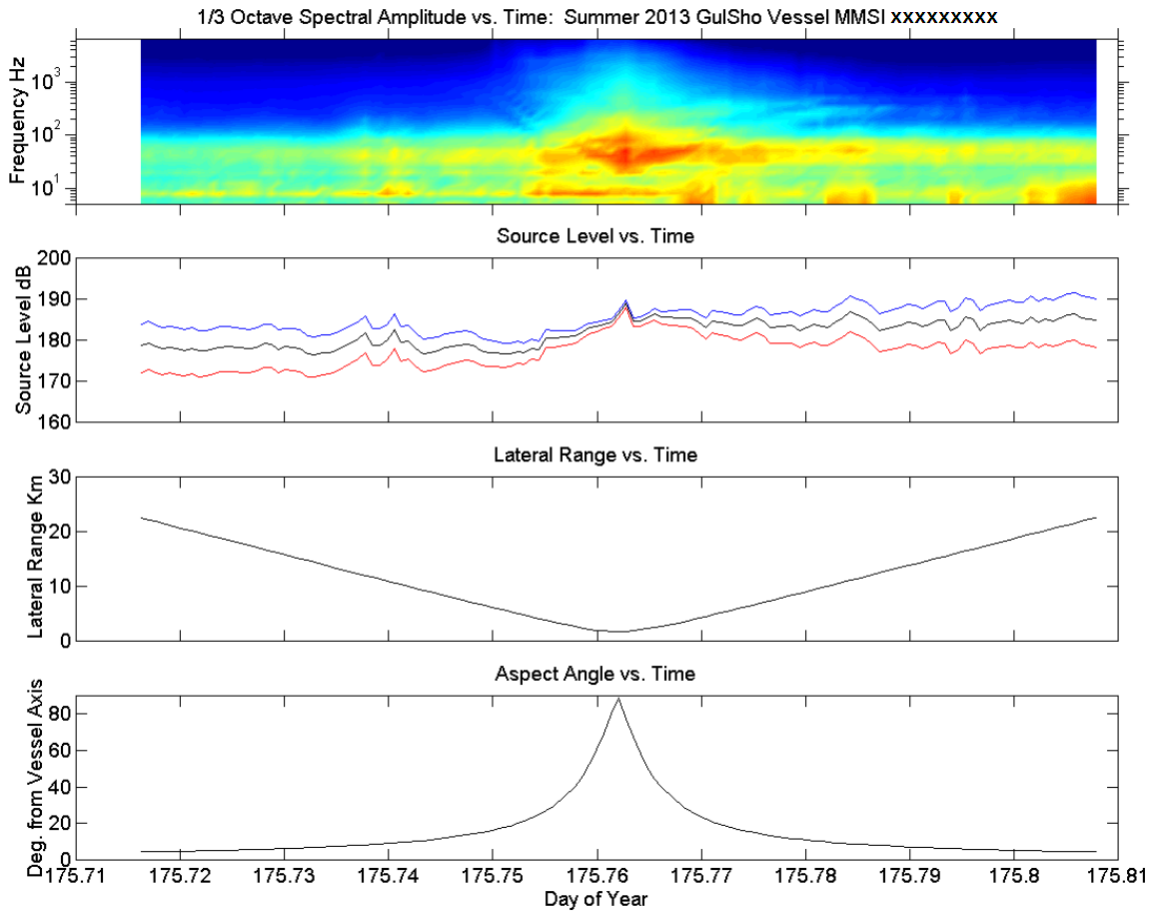

Figure 16. Vessel 1/3 octave acoustic spectral levels observed at GulSho mooring as a function of AMAR time (1st plot). Derived vessel acoustic source levels in dB re 1 μPa^2 @ 1 m using TL dependencies of 10.0 log (slant range) in red, 15.5 log (slant range) in black, and 20 log (slant range) in blue vs. time (2nd plot). Vessel lateral range (3rd plot) and observation angular aspect relative to the surface projection of the mooring (4th plot) vs. AMAR time. Vessel was *VESSEL "H"* (MMSI # xxxxxxxxx), average speed 11.04 knots, with closest approach 1.720 km lateral range at DOY 175.76198.

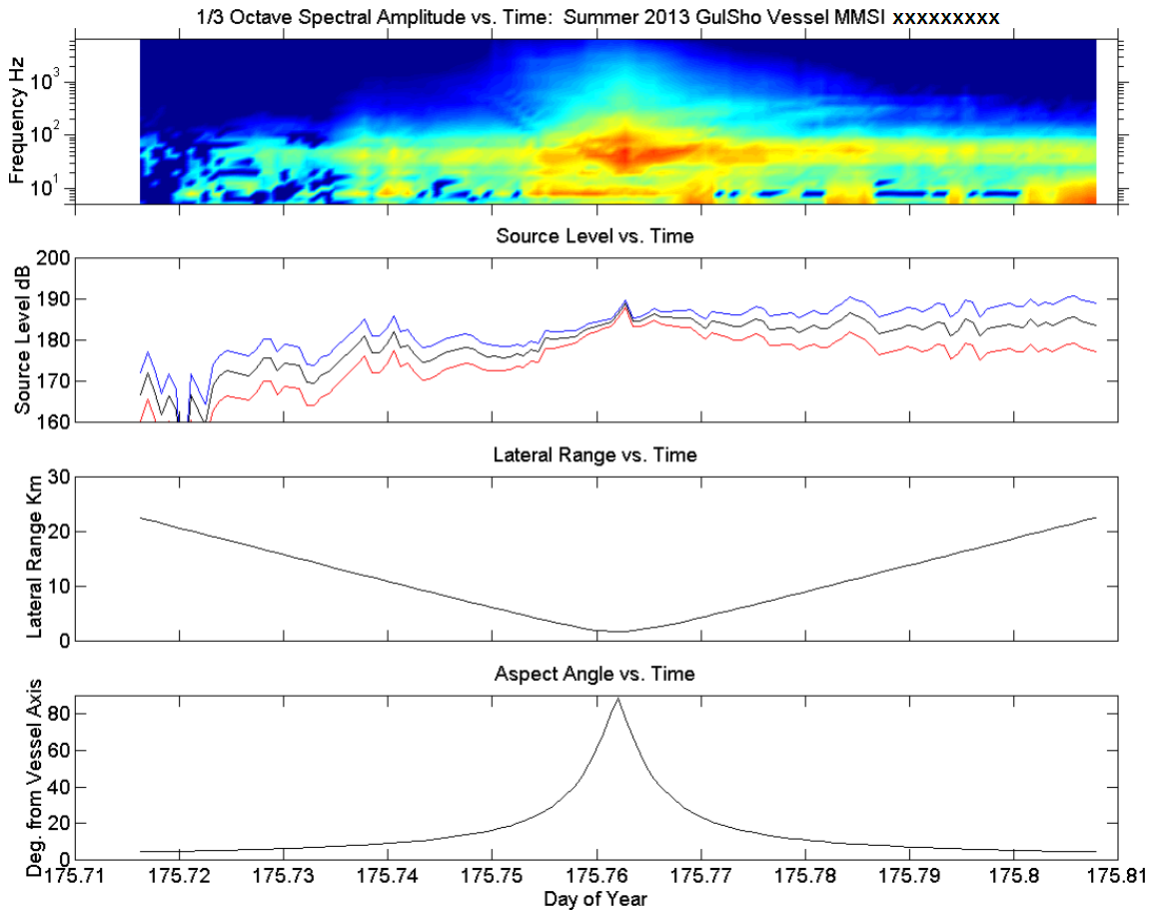

Figure 17. The same plots as in Fig. 16 except that the estimated ambient noise background obtained by averaging over the first 10 spectral estimates has been initially subtracted.

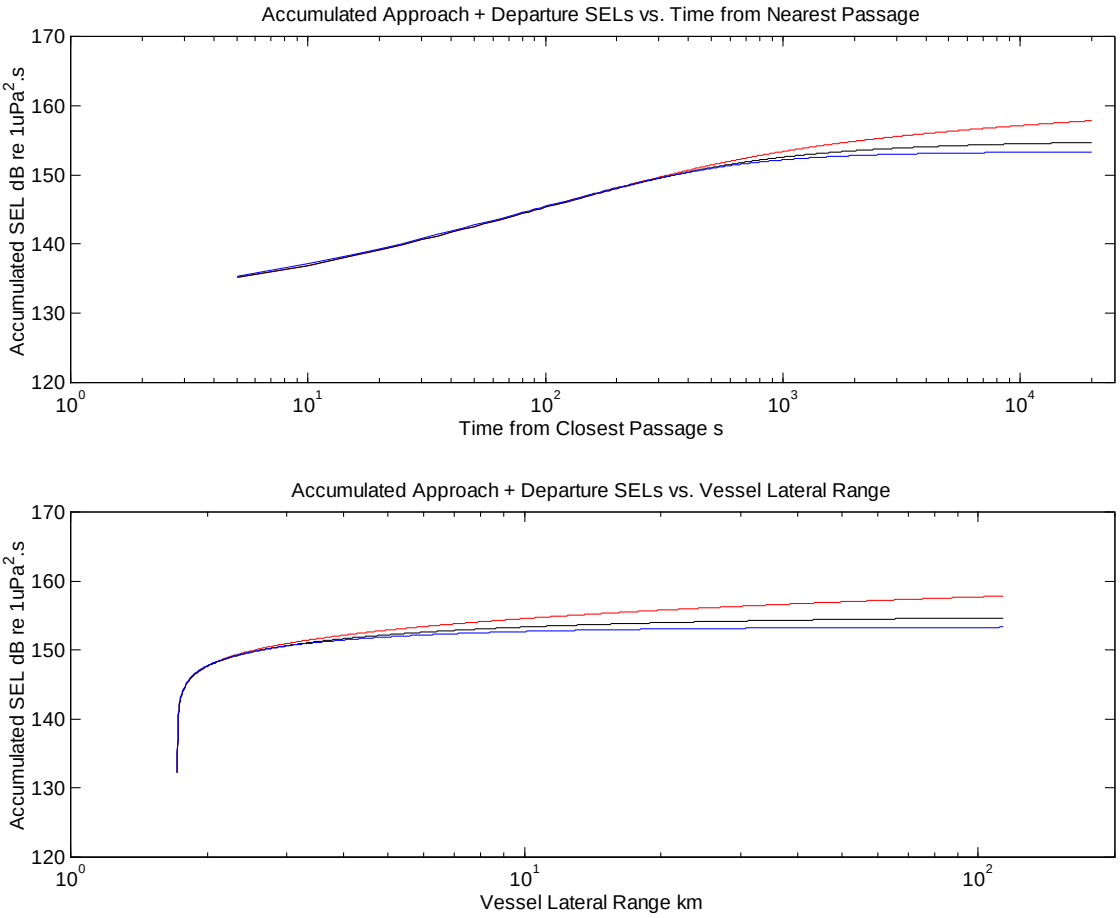

Figure 18. Mooring receiver theoretical cumulative SEL vs. time from closest passage (top) and theoretical cumulative SEL vs. vessel maximum lateral range (bottom) computed for *VESSEL "H"* (MMSI # xxxxxxxxx), transect passing near GulSho on 25 June 2013. Curves are computed assuming 10 log R (red), 15.5 log R (black) and 20 log R (blue) slant range dependencies.

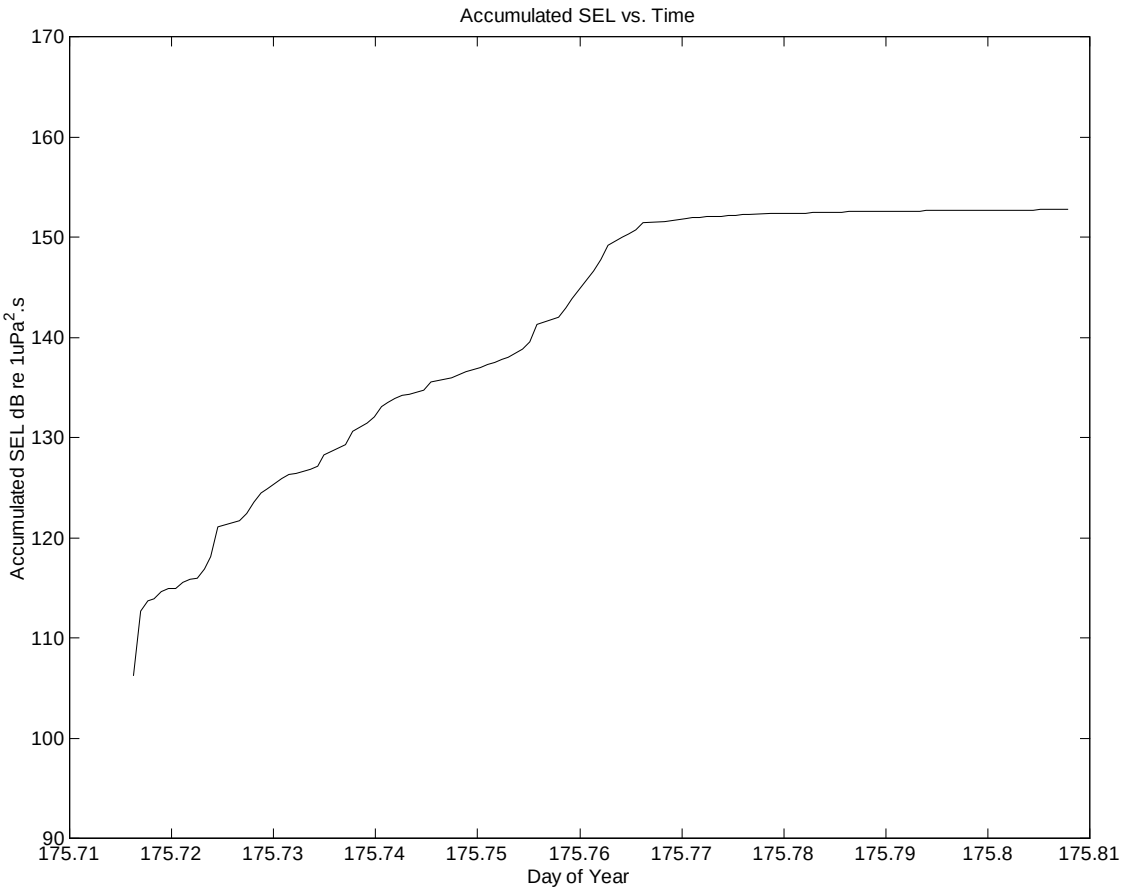

Figure 19. Experimentally computed SEL for *VESSEL "H"* (MMSI # xxxxxxxxx) passage of GulSho on 25 June 2013, utilizing successive 1/3 octave spectral estimates and the identical noise subtraction procedure and the identical considered spectral sub-range as used in the estimation of source levels. Vessel passage closest approach occurred at DOY 175.76198. SEL integration time extends from DOY 175.71623 to DOY 175.80789 corresponding to 3953 s prior to closest passage to 3967 s post closest passage.

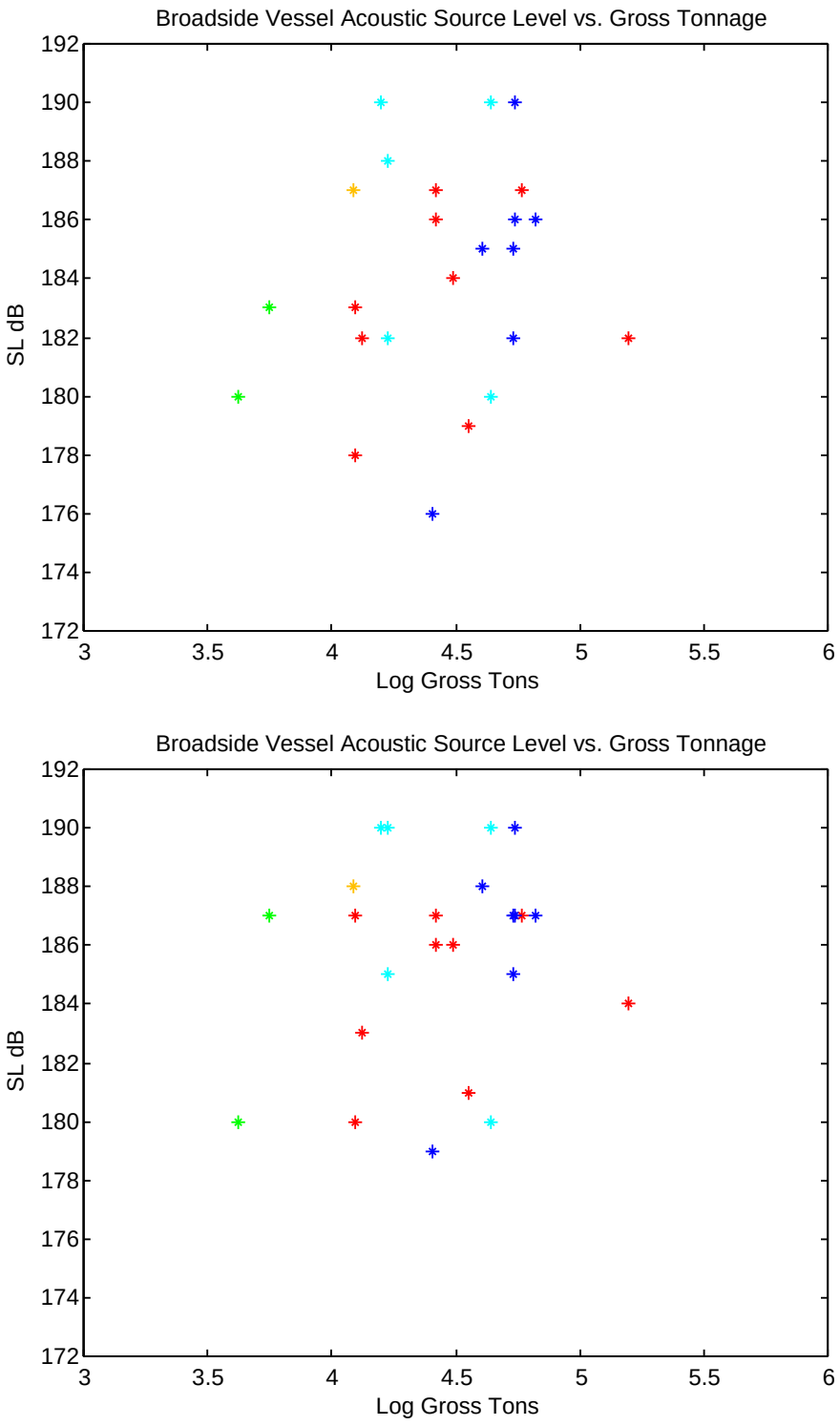

Figure 20. Vessel source level vs. vessel gross tonnage for all three AMAR stations combined assuming (top) 15.5 log R and (bottom) 20 log R slant range propagation corrections. Vessel types are colour coded: Blue – container vessels, green – dry cargo, cyan – bulk carriers, red – tankers, and orange – other types (cable vessel).

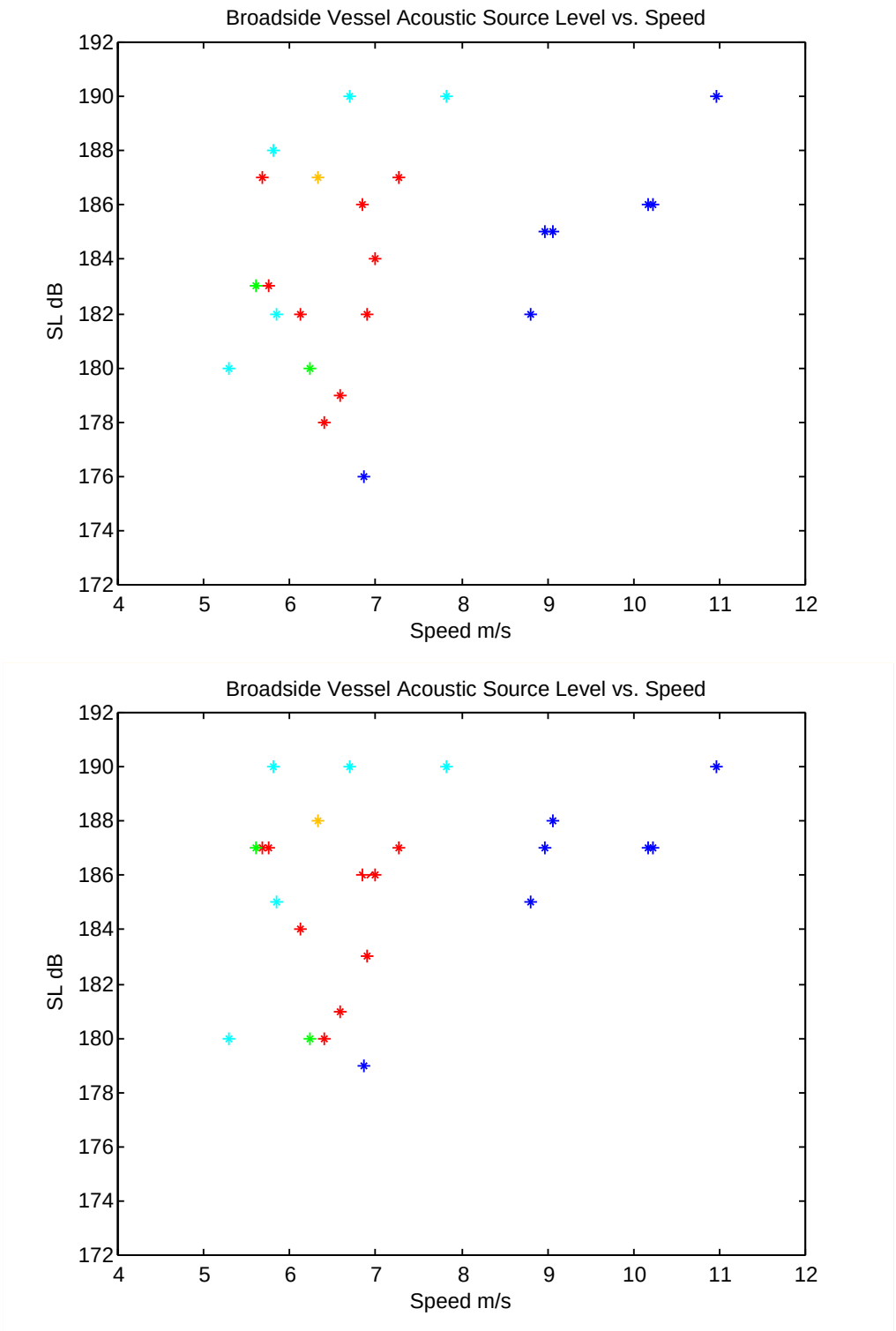

Figure 21. Vessel source level vs. vessel speed for all three AMAR stations combined assuming (top) 15.5 log R and (bottom) 20 log R slant range propagation corrections. Vessel types are colour coded: Blue – container vessels, green – dry cargo, cyan – bulk carriers, red – tankers, and orange – other types (cable vessel).

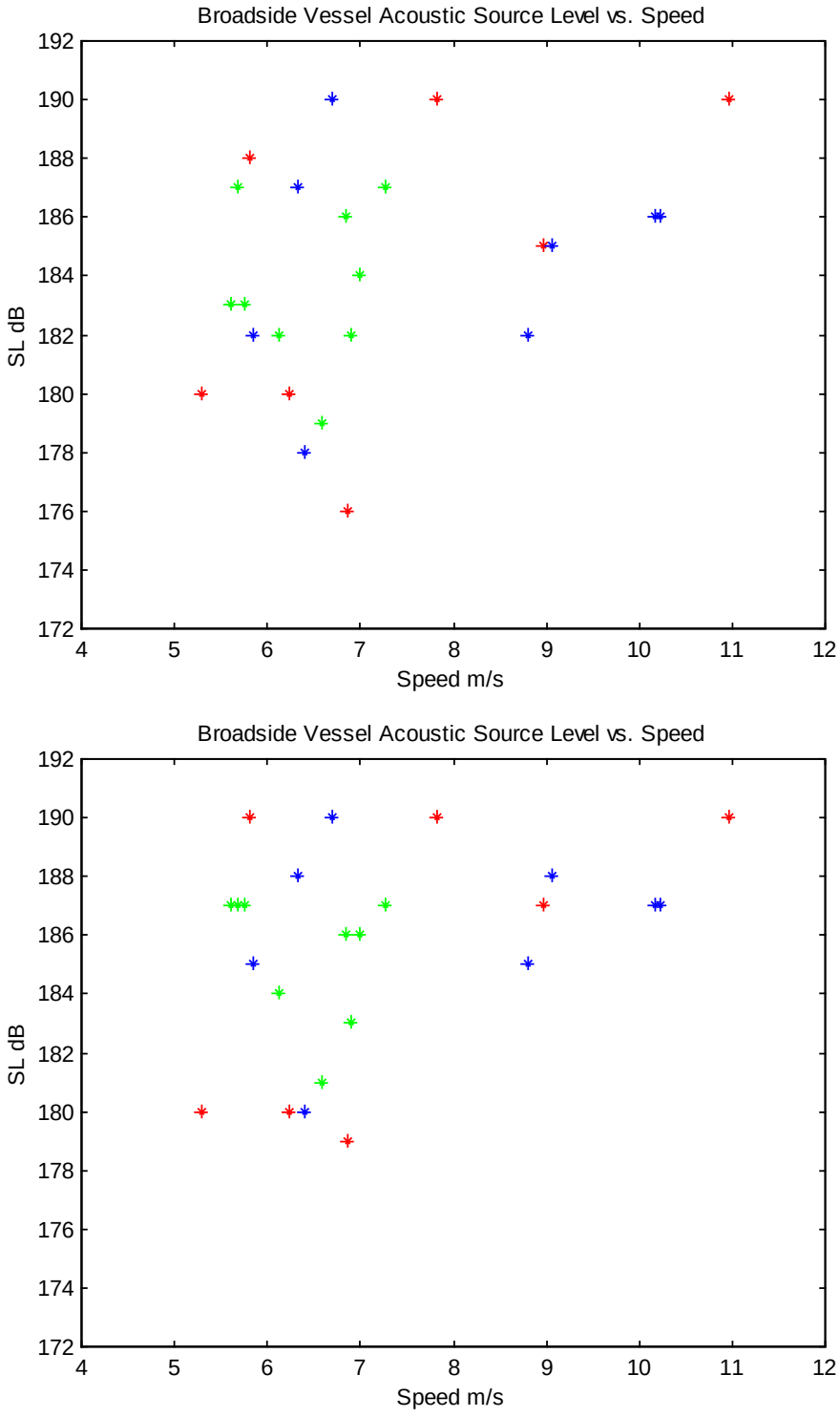

Figure 22. Vessel source level vs. vessel speed for three AMAR stations assuming (top) 15.5 log R and (bottom) 20 log R slant range propagation corrections. AMAR stations are colour coded: Red – MidGul, green – GulSho, and blue - ShoHald.

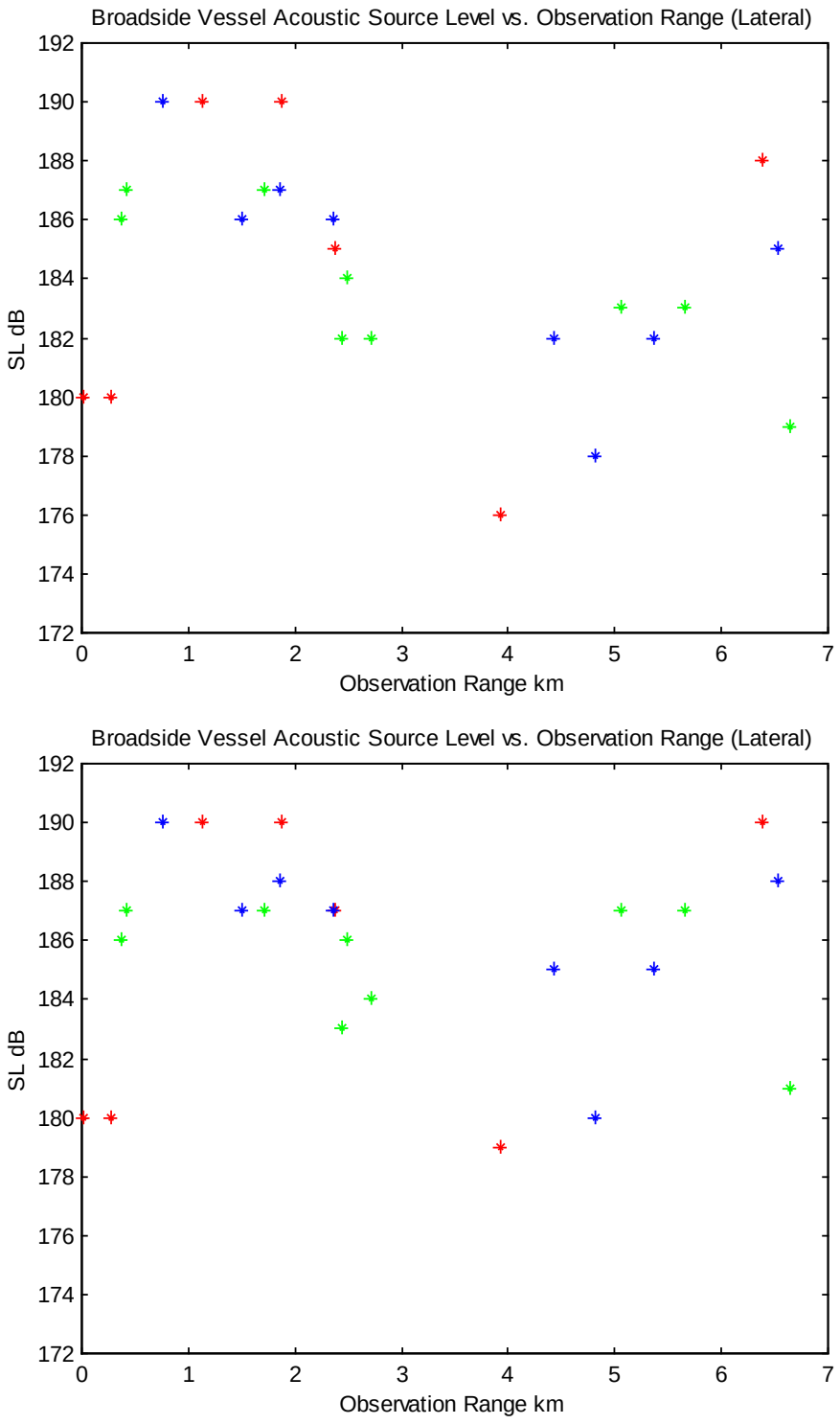

Figure 23. Vessel source level vs. lateral observation range for all three AMAR stations combined assuming (top) 15.5 log R and (bottom) 20 log R slant range propagation corrections. AMAR stations are colour coded: Red – MidGul, green – GulSho, and blue - ShoHald.

A1. APPENDIX 1: INTERFENCE FRINGE ANALYSES IN THE DETERMINATION OF VESSEL PASSAGE

A1.1. GENERAL

Broadband vessel passage sonograms, i.e. high time x frequency resolution acoustic spectrogram sections, obtained from the AMAR moored acoustic receiver/recorders often display systematic patterns of alternating high and low amplitude spectral fringes superimposed upon the otherwise slowly variant vessel noise spectral amplitudes. Successive fringes at any instant in time are observed to be nearly equi-spaced in the frequency domain and when isolated fringes are observed over an extended time interval their attendant acoustic frequencies tend to minimize at the time of closest vessel approach to the receiver. While experimentally observed vessel passage sonogram characteristics are invariably more complex than those predicted by the simplest theoretical models, their principal characteristics can be explained in terms of first-order acoustic interference effects arising from multi-path propagation from the vessel source to the moored receiver; namely, interference between the direct path vessel-to-receiver noise signal and both a) the vessel's water surface reflected signal (the classic Lloyd-mirror effect) and b) the vessel's first bounce bottom reflected signal. Sonogram sections employing minimal frequency and time domain smoothing allow phase interference effects between direct and reflected path signals to be readily visible when the vessel lies within a distance range from the mooring that the dominant multi-path arrivals retain phase coherence and are few in number. Observations of these interference phenomena are important to our analyses of ship passages since they offer a technique for establishing fairly precise times of closest vessel passages from the acoustic observations alone and within their attendant acoustic time bases. Comparison with AIS or other independent observations of the same vessel passages permit AMAR recorder time bases (subject to drift) and AIS time bases (essentially UTC) to be compared and any accumulated clock drift for the AMAR recorders to be discerned and compensated as necessary.

A1.2. THEORY

Figure A1-1 displays the propagation geometry, with (vessel) acoustic source *S* situated at depth *ds*, a moored (AMAR) receiving hydrophone *M* at height *h* above a level sea bottom, and the surface projection of the shallow vessel source residing at lateral range *R* from the surface projection of the hydrophone. Line *SM* represents the direct source-receiver acoustic path while the two additional signal paths impinge upon and are reflected without loss from the ocean surface and the ocean bottom at grazing angles of α and β respectively. The sound speed *c* is assumed invariant within the water column. The ocean surface constitutes a pressure release boundary inducing a 180^0 phase shift on reflection, while the ocean bottom is assumed hard inducing no phase shift.

The source to mooring distance *SM* is given by

$$SM = \sqrt{(D - ds - h)^2 + R^2} \tag{1}$$

where D is the total water column depth.

Surface Reflections

For the case of surface reflection, the source to receiver path length, SM_S, is given by:

$$SM_S = \sqrt{ds^2 + a^2} \; + \; \sqrt{(d - h)^2 + b^2} \tag{2}$$

From similar triangles

$$\frac{a}{b} = \frac{ds}{D - h} \tag{3}$$

from which follows

$$\frac{a}{a + b} = \frac{a}{R} = \frac{ds}{D - h + ds} \tag{4}$$

or

$$a = R\frac{ds}{D - h + ds} \tag{5}$$

similarly

$$b = R\frac{D - h}{D - h + ds} \tag{6}$$

Substituting (5) and (6) in (2):

$$SM_S = \sqrt{ds^2 + \left(R\frac{ds}{D - h + ds}\right)^2} \; + \; \sqrt{(d - h)^2 + \left(R\frac{D - h}{D - h + ds}\right)^2} \tag{7}$$

The direct path signal and the surface reflection will arrive in phase if their path difference is an integral number of wavelengths (λ) plus a ½ wavelength - because of the surface induced phase inversion:

$$SM_S - SM = n\lambda + \tfrac{1}{2}\lambda \tag{8}$$

Therefore, for sound speed c the frequency of the n^{th} in-phase (bright) fringe, f_n, is given by:

$$f_n = (n + \tfrac{1}{2}) \frac{c}{SM_S - SM} \tag{9}$$

The constant frequency difference between successive bright fringes at a given source lateral range will be given by:

$$\Delta f = f_{n+1} - f_n = \frac{c}{SM_S - SM} \tag{10}$$

Bottom Reflections

Considering bottom reflections, the bottom reflection path length relation analogous to (2) is:

$$SM_B = \sqrt{(D - ds)^2 + p^2} + \sqrt{h^2 + q^2} \tag{11}$$

Again from similar triangles this reduces to an expression analogous to (7):

$$SM_B = \sqrt{(d - ds)^2 + \left(R \frac{D - ds}{D - ds + h}\right)^2} + \sqrt{h^2 + \left(R \frac{h}{D - ds + h}\right)^2} \tag{12}$$

Since there is no phase inversion accompanying the bottom reflection the bright fringe condition of phase reinforcement will be:

$$SM_B - SM = n\lambda \tag{13}$$

$$f_n = \frac{n\ c}{SM_B - SM} \tag{14}$$

$$\Delta f = \frac{c}{SM_B - SM} \tag{15}$$

A1.3. APPLICATION TO AMAR MOORINGS

Our summer 2013 AMAR mooring hydrophones were deployed about 60 m above bottom in water depths of roughly 1500 m.[10] For the propeller or hull-radiated noise from large commercial vessels a typical source depth might be 10 m. Considering the case of surface reflections with the vessel **directly over the receiver**, the lowest frequency in-phase fringe will occur at 36.75 Hz assuming c = 1470 m/s, with successive in-phase fringes appearing at frequency increments of 73.5 Hz. For the corresponding bottom reflections, the first in-phase fringe will occur at 0 Hz with successive in-phase fringes at frequency increments of 12.25 Hz. In both cases, dark out-of-phase fringes will occur at equal increments in the frequency domain, their frequencies located at the arithmetic mid-points between successive in-phase fringe frequencies, with one dark fringe water surface reflection approaching zero frequency. The resultant computed phase effects vs. vessel lateral range for surface and for bottom reflections utilizing our quoted mooring parameters and sound speed are illustrated in Figs. A1-2 and A1-3, respectively. Note in both cases the bottoming-out of individual fringe frequencies (vertical axis) as the vessel passes directly overhead. Since individual (i.e. corresponding to a specific value of n) fringe frequencies rise monotonically with source lateral range, the same bottoming-out of the fringe frequencies will be observed at minimum lateral range for vessels proceeding on straight-line courses but not transiting directly over the mooring. This affords a potentially fairly precise technique for determining when, within the acoustic time base (i.e. AMAR recorder) itself, a vessel is at minimum observation range using sonogram observations alone without reference to any independent external vessel tracking methodology and necessary knowledge of the cumulative offset between the external and acoustic time bases.

Our experience from the Summer 2013 AMAR dataset is this technique works reasonably well for vessels known to pass (from AIS tracking) within several km of the moorings. For large commercial vessels it would appear that only the bottom reflection interference effects are clearly observed at the ranges chosen for intensive analysis, any phase-coherent Lloyd-mirror effects from surface reflections being difficult to observe and perhaps largely, if not entirely, obscured by the vessel wake and/or the presence of the ship hull. At lateral ranges exceeding 5 - 7 km the technique breaks down, the fringes becoming non-visible perhaps because simple geometries with a minimal number of high amplitude ray-paths can no longer be assumed even as a first approximation together with a probable general loss in signal coherence from a number of different range-dependent real-ocean processes. Even when interference effects are clearly observed, real slopping or undulating seafloors will introduce some degree of systematic error – a clear limitation to the technique.

A1.4. ADDITIONAL MODELLING

Some additional work has been conducted using non-ray based P.E. simulations of propagation from vessels to our moorings incorporating: 1) A flat bottoms 2) Realistic sound speed profiles 3) Realistic bottom reflectivities. It is known that the P.E.

[10] These numbers are approximate. For the specific moorings of (main text) of Table 1 and our P.E. modelling we choose a slightly deeper water depth but the 1500 m approximate water depth is sufficiently accurate for illustrative purposes.

modelling techniques, including those using Padé series approximations break down in modelling bottom reflections at high angles of incidence. Therefore, P.E. techniques may be poorly suited to exploring fringe generation for vessels passing very close to an AMAR mooring. Although detailed results are not presented in this report, on use of the RAM P.E. model configured for enhanced performance at high angles of incidence, it was observed that the main characteristics of fringe generation by the simple geometric ray model seem to be upheld. Also, on examining plots of vessel-to-mooring acoustic TL vs. vessel lateral range it appears that interference fringe generation by bottom reflection is the dominant (i.e. most clearly visible) mechanism at 100 Hz and below while fringe generation by surface reflection tends to become dominant at 1000 Hz and above. The very simple P.E. techniques employed **did not** examine ship radiator departure from a point source, wake absorption, or surface wave facet scattering – effects likely important in the real world.

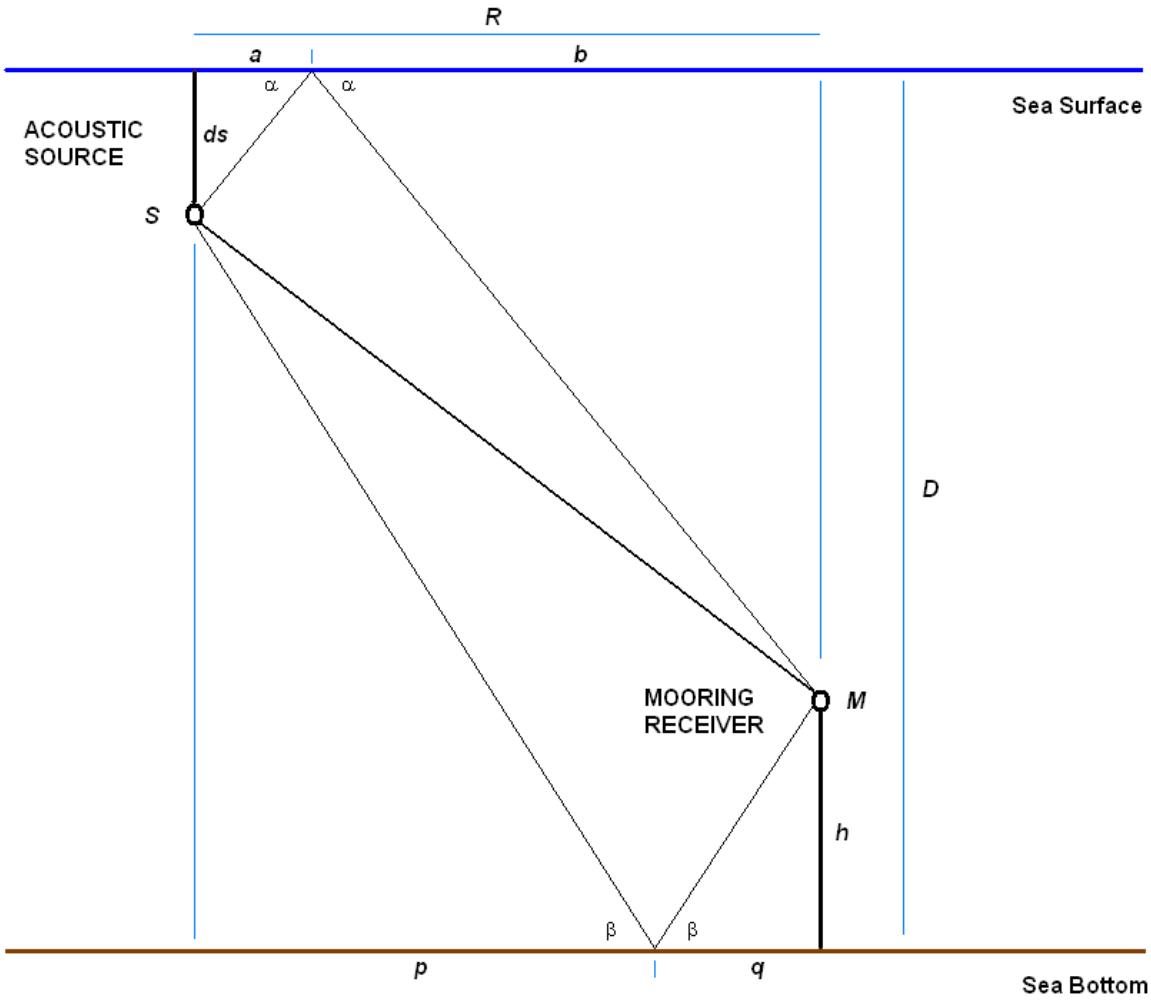

Figure A1-1. Acoustic propagation path geometries from acoustic source to moored acoustic receiver.

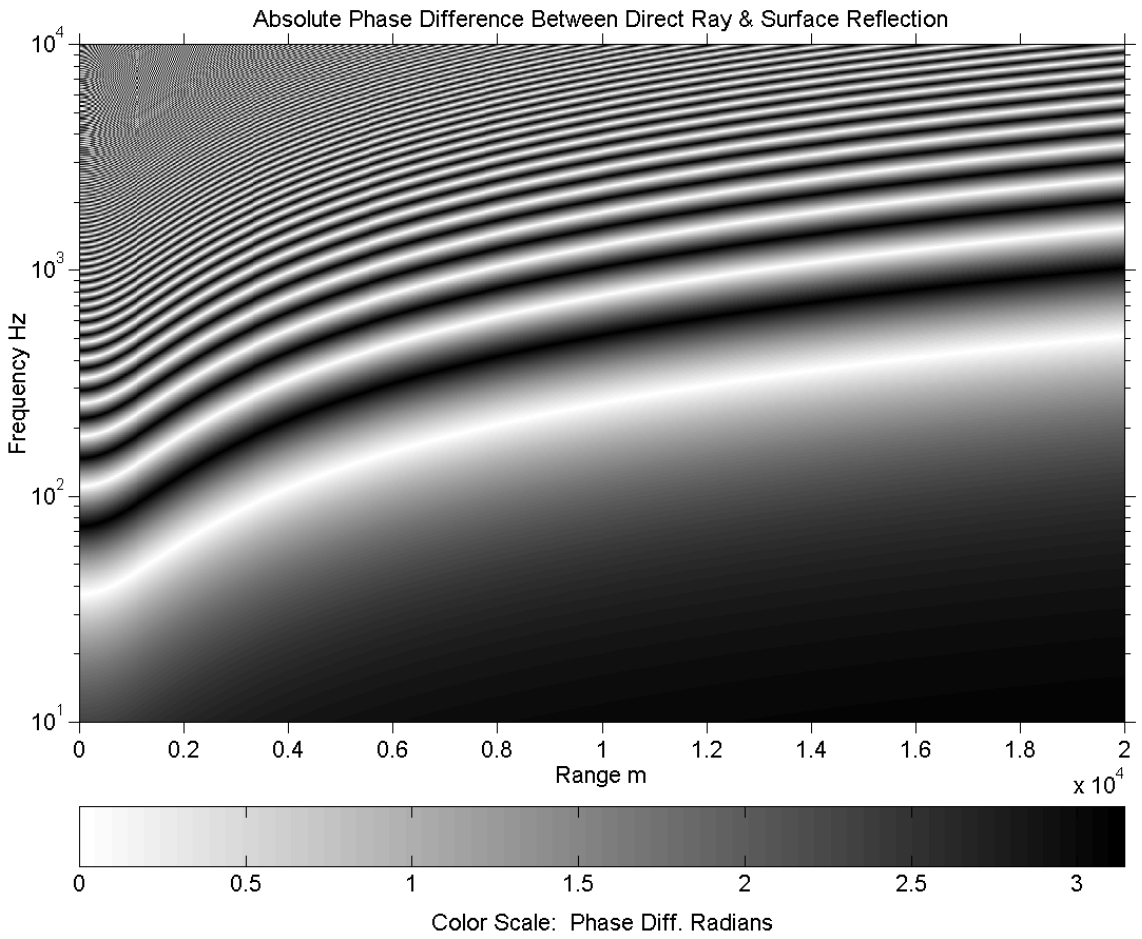

Figure A1-2. Absolute phase difference in radians between direct path and *surface* reflected signals at acoustic mooring. Parameters: Water depth = 1500 m, source depth = 10 m, and hydrophone height above bottom = 60 m.

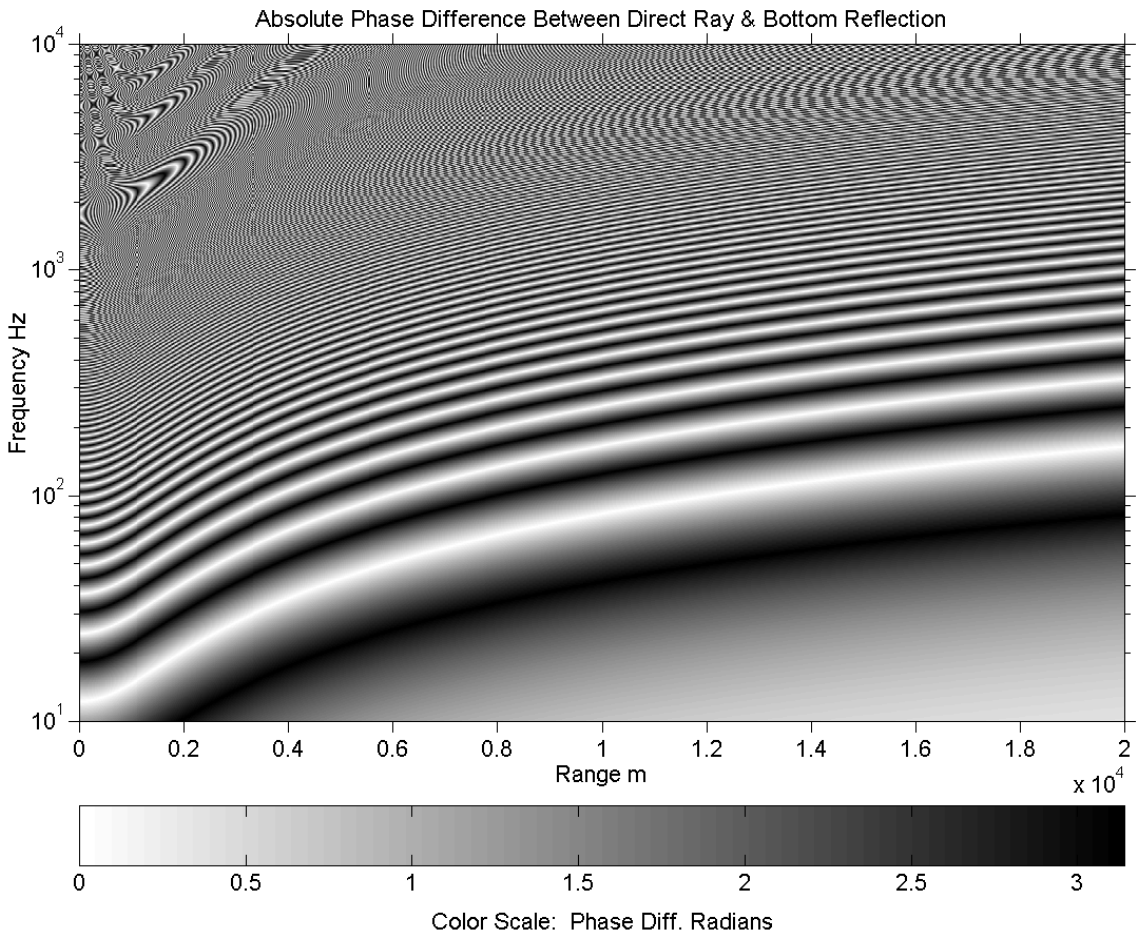

Figure A1-3. Absolute phase difference in radians between direct path and *bottom* reflected signals at acoustic mooring. Parameters: Water depth = 1500 m, source depth = 10 m, and hydrophone height above bottom = 60 m.

A2. APPENDIX 2: SOUND EXPOSURE LEVELS FOR VESSEL PASSAGE

The cumulative sound exposure level (SELs) for an entire ship passage or a portion thereof is defined as the decibel form (commonly) time integral of the squared RMS sound pressure level over the relevant time interval t_1 to t_2. For a complete vessel passage the time interval may be viewed as extending from essentially - ∞ to + ∞.

$$SEL_{dB} = 10\log\int_{t_1}^{t_2} P_{S\,RMS}^2 .dt$$

On considering the sonar equation with decibel source-to-receiver decibel TL defined as a +ve quantity:

$$SPL_{dB} = 10\log P_{S\,RMS}^2 = SL_{dB} - TL_{SR\,dB}$$

Further considering the inferred logarithmic dependencies of transmission loss (*TL*) on source to receiver slant range R_{sl} (main text) to be of general form (section 2.3.1 main text)

$$TL_{SRdB} = a\log(R_{sl}/R_0) + b$$

where the reference range, R_0, of 1 m has been added for dimensional consistency, SEL_{dB} can be written:

$$\begin{aligned} SEL_{dB} &= 10\log\int_{t_1}^{t_2} P_{S\,RMS}^2 .dt = 10\log\int_{t_1}^{t_2} 10^{(SL_{dB}-TL_{SRdB})/10}.dt \\ &= 10\log\int_{t_1}^{t_2} 10^{(SL_{dB}-a\log(R_{sl}/R_0)-b)/10}.dt \\ &= SL_{dB} - b + 10\log\int_{t_1}^{t_2} \left(R_{sl}/R_0\right)^{-a/10}.dt \end{aligned}$$

If the considered vessel is travelling at constant speed, *v* on a straight line course in a flat earth geometry; defining *t* = 0 to be the time origin at the point of closest passage at **lateral** range, R_c, considering the source depth, d_s, and receiver mooring depth, d_m, the source-to-receiver slant range at elapsed time, t_p, measured from time of closest passage will be:

$$R_{sl} = \left(\left(d_m - d_s\right)^2 + v^2 t_p^2 + R_c^2\right)^{1/2}$$

This yields a cumulative SEL from *t* = 0 to time t_p:

$$SEL_{dB}(t_p) = SL_{dB} - b + 10\log \int_{t_1=0}^{t_2=t_p} \left(\left((d_m - d_s)^2 + v^2 t^2 + R_c^2 \right) / R_0^2 \right)^{-a/20} .dt$$

Investigation of this integral in the case of a = 10, characterizing pure cylindrical spreading, shows that integral becomes infinite as $t_2 \rightarrow \infty$. This means that the SEL will accumulate to an indefinitely high value for a vessel passage evaluated to an indefinitely long duration post passage. In other words, it is impossible to place an upper limit on a SEL for a vessel passage extending to infinite time – i.e. no time or distance limit relative to closest passage can be defined beyond which contributions to the passage SEL become negligible, or even finite. Fortunately, the integral does appear to remain finite for $t_2 \rightarrow \infty$ for all $a > 10$, although convergence will be slow for values of a only slightly exceeding 10. In these cases vessel sound arriving from very long ranges cannot be ignored in arriving at a realistic SEL. In reality, there is reason to believe that a is range dependent and probably characterized by values not be far from 10 at ranges of many 10's of km (i.e. cylindrical spreading finally becomes dominant beyond some range). Small but finite SEL contributions from the multitude of vessels at very long range encompassing virtually the entire extents of broad ocean basins may be related to the existence of the well-recognized non-vessel-specific, shipping noise background although this is a slightly different topic. Our earlier P.E. modelling results (main text) utilizing a level bottom possessing realistic acoustic properties and a realistic water column sound speed profile etc. suggested a values in the numeric range of 15 – 20 out to distances of 20 km or so.

For the specific case of a = 20, a value which some investigators have preferred and not greatly at variance with our P.E. modelling, a simple closed form analytical expression can be written:

$$SEL_{dB}(t_p) = SL_{dB} - b + 10\log \int_{t_1=0}^{t_2=t_p} \left(\left((d_m - d_s)^2 + v^2 t^2 + R_c^2 \right) / R_0^2 \right)^{-1} .dt$$

$$= SL_{dB} - b - 20\log R_0 + 10\log \left[\frac{1}{v\sqrt{(d_m - d_s)^2 + R_c^2}} \tan^{-1} \frac{vt}{\sqrt{(d_m - d_s)^2 + R_c^2}} \right]_{t_1=0}^{t_2=t_p}$$

Which for R_0 = 1 m reduces to:

$$SEL_{dB}(t_p) = SL_{dB} - b + 10\log \left(\frac{1}{v\sqrt{(d_m - d_s)^2 + R_c^2}} \tan^{-1} \frac{vt_p}{\sqrt{(d_m - d_s)^2 + R_c^2}} \right)$$

If $t_p \rightarrow \infty$ the above expression remains finite:

$$SEL_{dB}(t_p \to \infty) = SL_{dB} - b + 10\log\left(\frac{\pi}{2v\sqrt{(d_m - d_s)^2 + R_c^2}}\right)$$

We have only considered the departure leg of ship passage. If we include both the approach and departure legs and if both legs are symmetric about closest passage, the decibel SEL increases by 3 dB.

What fraction of the total vessel passage SEL is in theory accumulated within a given vessel range of the mooring or during a given time interval about closest passage? Consider the linear form, SEL_L, of the general *SEL* expression:

$$SEL_L(t_p) = 10^{SEL_{dB}(t_p)/10}$$
$$= 10^{(SL_{dB}-b)/10} \bullet \left(\frac{1}{v\sqrt{(d_m - d_s)^2 + R_c^2}} \tan^{-1} \frac{vt_p}{\sqrt{(d_m - d_s)^2 + R_c^2}}\right)$$

The fraction of the total SEL of passage accumulated within a given elapsed time post-passage, $F_{SEL}(t_p)$, will be given by:

$$F_{SEL}(t_p) = SEL_L(t_p) \Big/ SEL_L(t_{p\to\infty}) = \frac{2}{\pi} \tan^{-1} \frac{vt_p}{\sqrt{(d_m - d_s)^2 + R_c^2}}$$

Consider the main text example of the tanker *VESSEL "M"* travelling at 11.91 kts (6.13 m/s) with a closest passage lateral range to the GulSho mooring of 2.713 km. In Fig. A2-1 are plotted the fractions of total passage SEL accumulated, in theory, as a function of time from nearest vessel passage, and as a function of vessel lateral range from the mooring. It is noted that 90% of the passage sound exposure is acquired within approx. 3000 s of the time of nearest passage while the vessel is within about 20 km lateral range of the mooring. About 60% of the total exposure is acquired within a lateral range of about 5 km. Notice that the fraction as a function of accumulation time is dependent on both the vessel speed and the geometry of passage, while the fraction as a function of lateral range is dependent on the geometry alone.

It is important to remember that the above explored case for a range-independent $a = 20$, may not, and probably is not, representative of real sound propagation at ranges beyond several 10's of km. Actual real-world sound exposures accumulated at vessel ranges well in excess of 20 km could be (and likely are) greater than those computed under the above assumption of $a = 20$. Nevertheless, regardless of the choice of a, the original SEL integral does remain finite for all finite t_p, and consequently SELs can be estimated, by numerical integration if required, for any time limited transit or time bounded portion of the transit provided the vessel source level can be extracted or is otherwise known[11].

[11] Since there is uncertainty regarding transmission loss behaviours at very long vessel ranges it is probably safer to numerically estimate accumulated SEL out to a given vessel range, for instance 10 km, than to state

Whether and under what conditions SEL estimation utilizing this methodology might be superior to SELs computed directly by the frequency and time integration of observed vessel spectral levels or, alternatively, time integration of the time domain squared pressure signal remain to be explored. Directly computed experimental SELs present the problem of distinguishing specific vessel noise from the fluctuating ambient background but possess the great advantage of dispensing with idealized assumptions about how TL varies with vessel range and with frequency. Nevertheless, theoretical SELs afford well constrained, easily explored insights as to how real-world SELs may depend on important parameters such as vessel passage range, vessel speed, and perhaps even changing aspect, etc. and this should probably constitute their main application.

what portion the limited range SEL constitutes of the total accumulated SEL for the vessel passage extending to infinity.

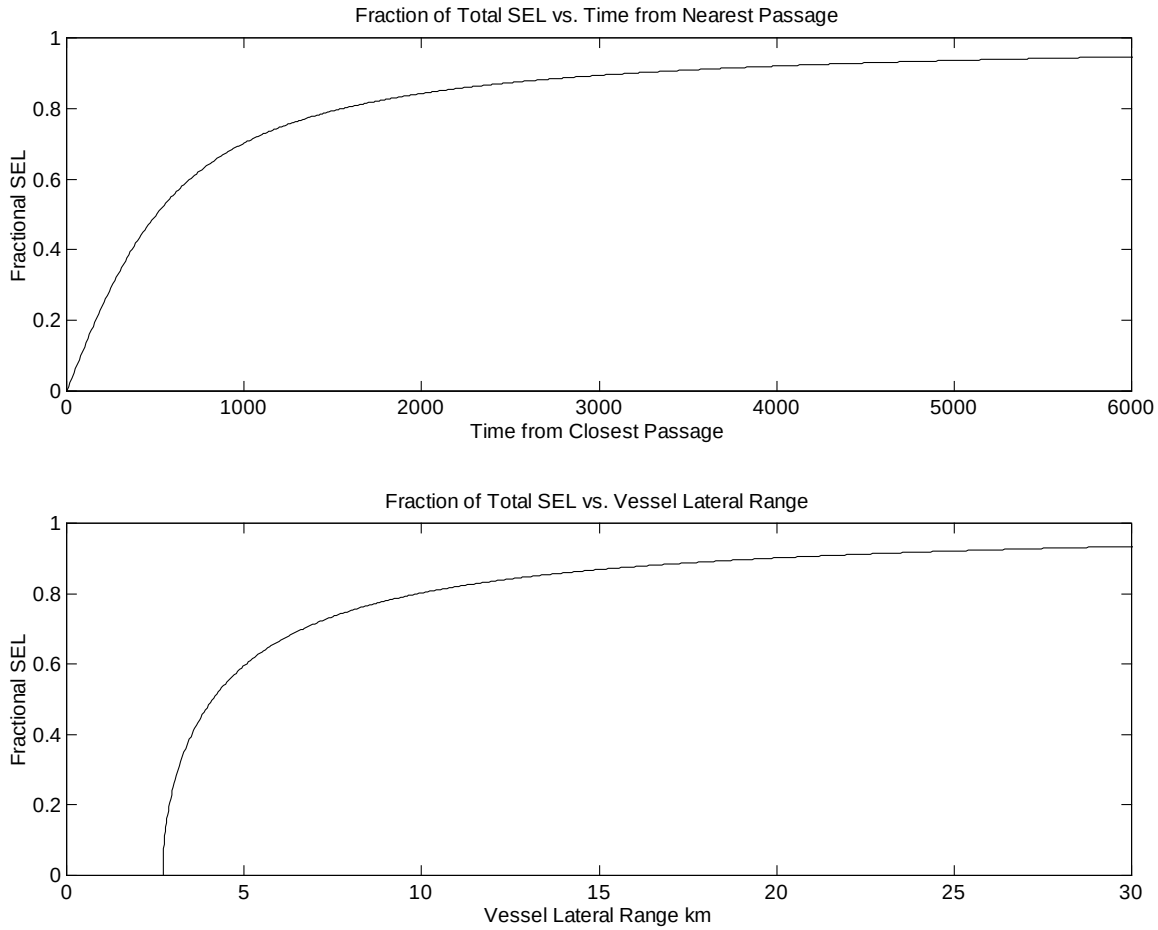

Figure A2-1. Fraction of total SEL theoretically accumulated within a given time of nearest vessel passage (top) and within a given vessel lateral range from the mooring (bottom) computed for the passage of tanker *VESSEL "M"* (MMSI # xxxxxxxxx) by the GulSho mooring on 23 June 2013.